www.MaterialsViews.com

Small is Smarter: Nano MRI Contrast Agents – Advantages and Recent Achievements

Zhenyu Gao, Tiancong Ma, Enyu Zhao, Dominic Docter, Wensheng Yang, Roland H. Stauber, and Mingyuan Gao**

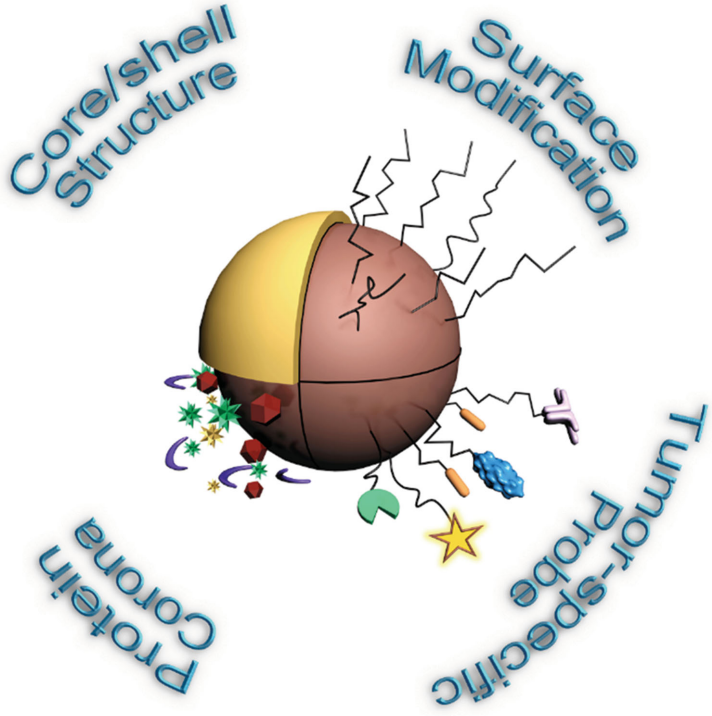

From the Contents

Many challenges for advanced sensitive and noninvasive clinical diagnostic imaging remain unmatched. In particular, the great potential of magnetic nano-probes is intensively discussed to further improve the performance of magnetic resonance imaging (MRI), especially for cancer diagnosis. Based on recent achievements, here the concepts of magnetic nanoparticle-based MRI contrast agents and tumor-specific imaging probes are critically summarized. Advances in their synthesis, biocompatible chemical and biofunctional surface modifications, and current strategies for further developing them into multimodality imaging probes are discussed. In addition, how engineered versus unintended surface coatings such as protein coronas affect the biocompatibility and performance of MRI nano-probes is also considered. To stimulate progress in the field, future strategies and relevant challenges that still need to be resolved in the field conclude this review.

small NANO MICRO

1. Introduction

Currently, there is an immense increase in the technical applications of nanoparticles (NPs) and also their (potential) use in medicine is steadily growing.[1,2] In the field of nanomedicine, NPs are increasingly considered as a promising type of agents useful for improving the efficacy of major diseases' theranostics.[3] Recent advancements in synthesis and the ability to effectively manipulate NPs' features, such as their physical, chemical, and biological properties, open up additional possibilities in rationally designing a new generation of nanoprobes as imaging agents and/or drug carriers.[4,5] Particularly, considerable progress in the development of magnetic NPs with engineered physicochemistry and tailored surface properties offers varieties of clinically relevant applications, such as magnetic resonance imaging (MRI), drug delivery, hyperthermia, and low cost in vitro diagnostics.[1,6–9]

For noninvasive diagnosis, MRI has been demonstrated as one of the most powerful imaging tools for visualizing the anatomical structures of soft tissues with cellular and even sub-cellular spatial resolutions.[10] It is now widely employed for the diagnosis of major diseases such as tumors, cardiovascular and cerebrovascular diseases,[11] yet the sensitivity for differentiating the malignant tissues and healthy tissues remains to be improved. Therefore, developing advanced MRI contrast agents has become one of the urgent tasks for further improving the efficacy of MRI diagnosis.

MRI is in principle achieved by detecting the relaxation signals of (water) proton spins, in a strong magnetic field excited by radiofrequency waves, with the aid of a magnetic gradient for spatially differentiating water protons within human body.[12] The relaxation of proton spins to their equilibrium states occurs via two processes, namely longitudinal relaxation characterized by relaxation time T_1, and transverse relaxation characterized by relaxation time T_2. Chemical agents that can speed up the recovery of longitudinal relaxation leading to increased T_1 signal intensity are called as T_1 contrast agents or positive contrast agents, while those can accelerate the transverse relaxation giving rise to hypointensive T_2 signal are called as T_2 contrast agents or negative contrast agents.[12]

Until now, the clinical T_1 MRI contrast agents are mainly chosen from gadolinium-based small molecular complexes that show several disadvantages with respect to tumor diagnosis, 1) the small molecular complexes exhibit no tumor specificity, 2) the rapid renal clearance potentially put the patients with poorer renal function at a risk of nephrogenic system fibrosis.[13] The clinical T_2 contrast agents such as Feridex as well as those at different stages of clinical trials are mainly magnetic iron oxide NPs coated with different types of biocompatible polymers. Unfortunately, the production of Feridex has been ceased. The possible reason is that it largely taken up by the liver after intravenous injection and is therefore used for detecting tumors and lesions in the liver.[14] But the low T_2 background signal of liver hampers its wide applications as T_2 contrast agents. Nevertheless, the enhanced permeability and retention (EPR) effects of malignant tumors and the enhanced uptake of nanometer-sized particles by disease-associated macrophages still greatly inspire the investigations of NP-based imaging agents and drug carriers.[15] In addition, the large surface-to-volume ratio offers a big room not only for drug-loading but also for designing of advanced target-triggering probes for revealing the tumor-associated microenvironment.[16] Most importantly, recent investigations have shown that through delicate control over the particle size, shape, and surface structure of NPs, the performance of magnetic NPs can be greatly improved for in vivo applications.[17]

Still, there are numerous challenges in the design and synthesis of advanced magnetic colloidal particles for biomedical applications. Hence, in the current review, we will describe 'classical' and novel strategies for the improved synthesis and surface modifications of magnetic NPs, and further discuss the challenges faced by NP-based MRI probes for the diagnosis of major diseases such as cancer, cardiovascular and neurological diseases by briefly summarizing the relevant progress.

2. Magnetic Nanoparticle Design and Controlled Synthesis Strategies

It has previously been demonstrated that the pharmacokinetic behaviors of NPs are strongly dependent on particle size and surface coating structure of NPs, apart from the significant dependencies of their physicochemical properties.[18] Delicate tuning over the particle size and clear defining of the particle surface coating structure remain challenging but extremely important for exploring in vivo applications of NPs. Meanwhile, developing multifunctional NPs is also biomedically relevant towards multi-modality imaging, drug delivery, and theranostics as well.[19,20] In addition, the large-scale synthesis of NPs with high reproducibility is also of the utmost importance for translating the lab particles to clinical drugs.[21,22]

2.1. Gadolinium-Based NPs

Among the trivalent lanthanide ions, Dy^{3+} and Ho^{3+} exhibit the highest magnetic moments benefiting from spin-orbit coupling.[23] Yet Gd^{3+} is most preferred for preparing T_1 contrast agents by forming Gd-chelates in comparison with the rest paramagnetic Ln^{3+} ions due to its largest number of unpaired

Z. Y. Gao, Prof. W. S. Yang
College of Chemistry
Jilin University
Changchun 130012, China
Z. Y. Gao, T. C. Ma, E. Y. Zhao, Prof. M. Y. Gao
Institute of Chemistry
Chinese Academy of Sciences
Bei Yi Jie 2, Zhong Guan Cun, Beijing 100190, China
E-mail: zhaoey@iccas.ac.cn; gaomy@iccas.ac.cn
D. Docter, Prof. R. H. Stauber
Department of Nanobiomedicine
ENT/University Medical Center of Mainz
Langenbeckstr. 1, 55101 Mainz, Germany

DOI: 10.1002/smll.201502309

electrons with parallel spin. More importantly, the spin-relaxation time of Gd^{3+} matches the Larmor precession frequency of protons within a suitable magnetic field.[2] Now there exist nearly ten different types of Gd-chelates serving as clinical T_1 contrast agents.[23–25] Similar to organic chelating agent, some inorganic compounds can firmly hold Gd^{3+} ions to prevent them from being dissolved in aqueous media even in NP forms.[18] In comparison with Gd-complexes, Gd^{3+}-containing inorganic NPs exhibit much higher longitudinal relaxivities r_1 per particle due to the presence of a large number of paramagnetic Gd^{3+} ions per particle. For example, a thin paramagnetic $NaGdF_4$ shell of 1.1 nm on 18.7 nm $NaYF_4$:Yb,Tm core presents a r_1 value per particle 5000 times higher than those of Gd^{3+}-complexes such as Gd-DTPA (Magnevist) and Gd-DOTA (Dotarem).[26] Most importantly, NPs exhibit much longer blood circulation time upon suitable surface modification, which is remarkably in favor of in vivo applications of these NPs especially for tumor imaging.[27] The additional benefit of using Gd-based NPs as T_1 contrast agents is that they can be doped with other types of Ln^{3+}, due to their close chemical properties, which provides great possibilities for rationally designing multifunctional Ln-NPs with unique magnetic and down-conversion/up-conversion luminescent NPs potentially useful for ultra-sensitive imaging applications.[28,29] Therefore, the synthesis of Gd-containing NPs for biomedical applications has recently become a very hot research field.

In general, the Gd-containing NPs potentially useful as T_1 contrast agents can roughly be classified into two categories, i.e., 1) NPs made up of stoichiometric inorganic compounds such as $NaGdF_4$, Gd_2O_3, GdF_3, $GdPO_4$, $GdVO_4$, $KGdF_4$, etc and these inorganic compounds are characterized by poor dissolubility in water, 2) Gd-doped rare earth NPs in suitable matrices such as $NaYF_4$, $NaLuF_4$, LnF_3, $LaPO_4$, $TbPO_4$, etc. Regarding the synthesis of these Gd-containing NPs, previous investigations suggest that non-aqueous synthetic methods are generally superior to aqueous synthetic methods with respect to morphology control over the resulting NPs.

Polyol-mediated synthesis is a suitable method for synthesizing a great variety of metal oxides NPs due to the excellent compatibility of the widely used solvent diethylene glycol (DEG) with a large range of organic and inorganic metal salts. In general, through the forced hydrolysis of metal ions in the presence of water and/or NaOH, nanometer-sized metal oxide NPs can be prepared at elevated temperatures.[30,31] This synthetic route was adopted for a few nanometer Gd_2O_3 particles that present higher longitudinal relaxivities r_1 than clinical T_1 contrast agent based on Gd-chlates.[32] The above-mentioned synthetic route is also applicable for synthesizing rare-earth doped Gd_2O_3 NPs with down-conversion[33] and up-conversion luminescent properties.[34]

In comparison with polyol synthesis, synthetic routes based on the pyrolysis of metal-organic compounds (thermal decomposition method) or replacement reactions taking place in organic solvents with high boiling points are suitable for producing different types of Gd-containing NPs apart from offering more effective measures for controlling the particle size due to the following reasons. Different from DEG that is expected as a surface capping agent, 1-octadecence (ODE) serving as a common non-coordinating solvent does not interfere with the particle growth. In addition, the latter offers a broader reaction temperature range that is favorable for effectively manipulating the particle nucleation and the following growth. More importantly, the exclusion of water as a Louis base from the reaction system is helpful for better regulating the particle growth kinetics apart from avoiding the unwanted hydroxides.

Yan and coworkers firstly reported highly monodispersed oleic acid capped LaF_3 NPs (16.0 ± 0.4 nm) obtained through the pyrolysis of $La(CF_3COO)_3$ in ODE at 280°C. Then, this thermal decomposition synthetic route was applied for synthesizing uniformly sized and shaped $NaGdF_4$ in oleic acid/oleylamine/ODE.[35] By the same method, through the pyrolysis of Gd-oleate as precursor, Colvin and coworkers

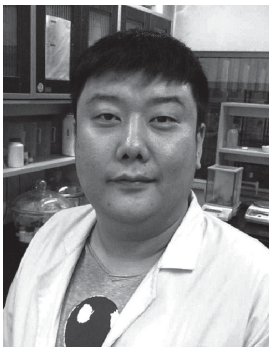

Zhenyu Gao holds a Master Degree in Physical Chemistry awarded in 2013 from the College of Chemistry, Jilin University. He is currently a PhD student co-supervised by Prof. W. Yang and Prof. M. Gao. His research interests include synthesis and applications of functional magnetic nanomaterials.

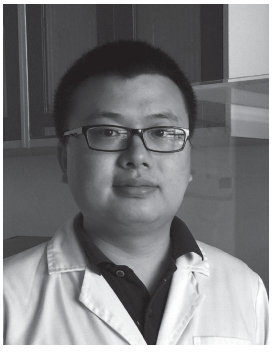

Enyu Zhao received his Master Degree in 2012 from the School of Pharmaceutical Sciences, Peking University. Since then, he has been working with Prof. M. Gao as a research assistant in the Institute of Chemistry, Chinese Academy of Sciences. His major research focuses on the biomedical applications of inorganic nanoparticles.

Mingyuan Gao is a Full Professor in the Institute of Chemistry, Chinese Academy of Sciences. He received his BSc (1989) and PhD (1995) in Polymer Chemistry and Physics at Jilin University. He worked as research assistant and associate in Germany from 1996 to 2002 and was an A. v. Humboldt fellow between 1996 and 1998. His research focuses on the synthesis as well as biological and biomedical applications of functional nanomaterials.

reported 2 nm Gd_2O_3 nanoplates stabilized by oleic acid. After overcoated with octylamine modified polyacrylic acid, the resulting water-dispersible Gd_2O_3 nanoplates presented a longitudinal relaxivity r_1 up to 47.2 mM^{-1} S^{-1} measured at 1.41 T, 10 times higher than Gd-DTPA, one of the typical clinical T_1 contrast agents.[36] By pyrolyzing gadolinium acetate in the presence of lithium ions, Murray and coworkers reported very uniform tripodal and triangular Gd_2O_3 nanoplates with optimized synthetic parameters such as reaction temperature and time. The relaxavity r_1 of Gd_2O_3 tripodal nanoplate was around 1.41 mM^{-1} S^{-1} determined at 9.4 T.[37] More importantly, this synthetic approach offers great opportunities for further synthesizing different types of magnetic/upconversion bifunctional NPs such as $NaGdF_4$:Yb,Er,[38–40] $NaGdF_4$:Yb,Ho, Gd_2O_3:Yb,Er, Gd_2O_3:Tb, Gd_2O_3:Eu,[37] etc.

Zhang and coworkers developed an alternative approach for producing high quality rare-earth NPs through replacement reactions taking place in non-polar high-boiling point ODE in 2008. They successfully obtained monodispersed β-$NaYF_4$:Yb,Er/Tm nanocrystals such as 21 nm spherical particles, 17 × 22 nm ellipsoidal particles, and 30 × 45 nm hexagonal plates through the replacement reaction between $LnCl_3$ and NH_4F taking place in the presence of NaOH, and disclosed the role of oleic acid (OA) ligand in regulating the particle size and morphology.[41,42] These early works arouse enormous research interests in synthesizing Gd-NPs with well-defined size and shape, and surface chemistry for further biomedical applications. For example, van Veggel and coworkers reported the size tunable synthesis of monodisperse β-$NaGdF_4$ NPs below 10 nm and obtained NPs of 2.5 nm, 4.0 nm, 6.5 nm, and 8.0 nm by fine tuning of reaction time and temperature. After the NPs were transferred into aqueous media by replacing the hydrophobic oleate ligand with polyvinylpyrrolidone, the resulting water soluble particles exhibited clear particle size dependence of r_1, i.e., smaller NPs show high ionic relaxivity values relative to the larger ones due to larger surface-to-volume (S/V) ratio, while the tumbling time increases as the NP size increases, leading to enhanced contribution of surface ions to r_1. Nevertheless, S/V remains a dominant factor in the above size regime.[43] Gao and coworkers further found out that the particle growth in a similar reaction system undergoes a size broadening process at 300 °C, followed by a size focusing process, which suggests that the Ostwald ripening process plays an important role in determining both particle size and size distribution. Through independently manipulating the particle nucleation and growth processes, they successfully obtained monodisperse $NaGdF_4$ NPs up to 20 nm.[44] Upon further surface ligand exchange, the resulting PEGylated $NaGdF_4$ NPs of 5.4 nm, 15.1 nm, and 19.8 nm, as shown in **Figure 1**, presented a nonmonotonic ionic r_1 against the particle size, e.g., 6.2 mM^{-1} s^{-1} (5.4 nm), 5.7 mM^{-1} s^{-1} (15.1 nm), and 8.8 mM^{-1} s^{-1} (19.8 nm) determined with a 3 T MRI scanner, different from the above-mentioned size-dependence of r_1. This may be because the tumbling effect for the particles close to 20 nm is stronger enough to counteract the S/V effect. By independently tuning the ratios of F^-:Ln^{3+} and Na^-:Ln^{3+}, they further achieved monodisperse magnetic/upconverting $NaGdF_4$:Yb,Er NPs with variable sizes (10–80 nm) and shapes (spherical particles, wheel-like particles, hexagonal plates), as shown in **Figure 2**.[18] Apart from bright green upconversion luminescence, as shown in **Figure 3**, the resulting $NaGdF_4$:Yb,Er NPs also presented r_1 value higher than Gd-DTPA, which enable them useful for constructing MR/optical dual-modalilty tumor imaging probes that will be discussed in following part of this review.[18,44] In addition, the above-mentioned synthetic route is very suitable for constructing core/shell-structured rare-earth NPs for further tailoring both magnetic and optical properties of Gd-containing NPs. For example,

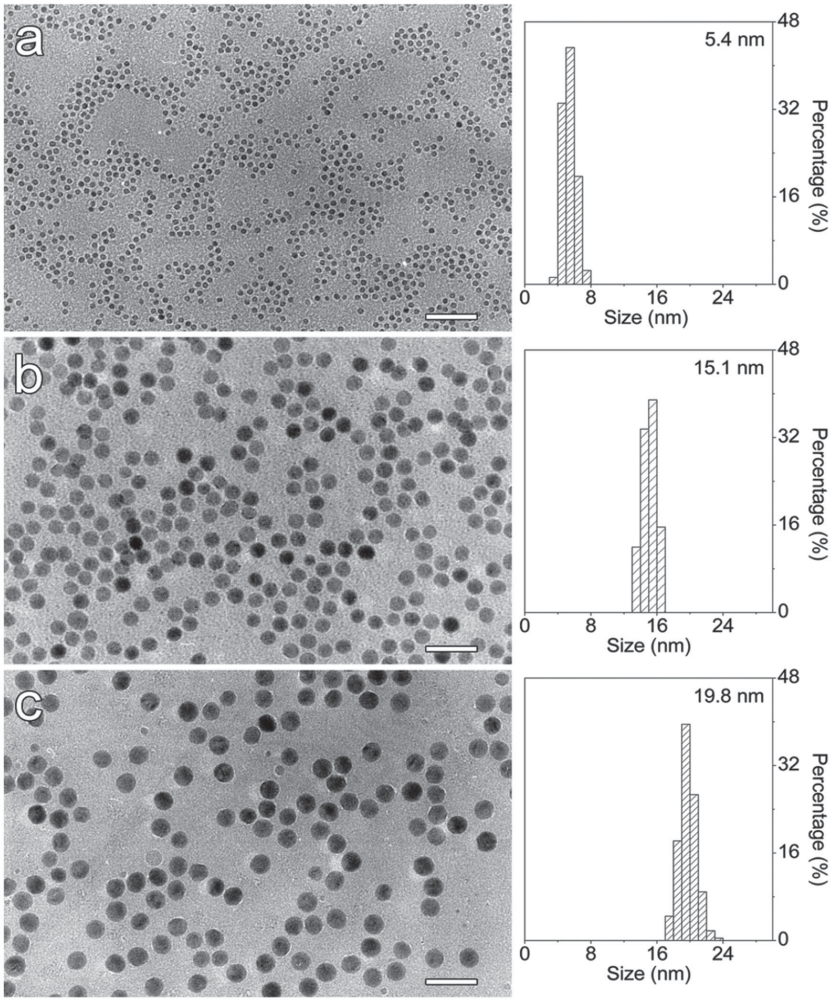

Figure 1. Transmission electron microscopy (TEM) images and histograms of PEGylated $NaGdF_4$ NPs of a) 5.4 nm, b) 15.1 nm, and c) 19.8 nm. The scale bars correspond to 50 nm. Reproduced with permission.[44] Copyright 2013, American Chemical Society.

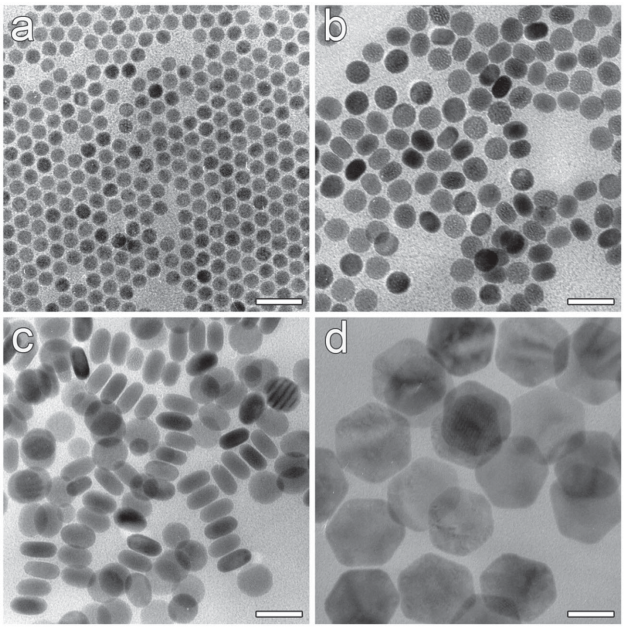

Figure 2. TEM images of $NaGdF_4$:Yb,Er NPs of a) 14.6 nm, b) 24.6 nm, c) 36.7 nm, and d) 82.3 nm. The scale bars correspond to 50 nm. Adapted with permission.[18] Copyright 2013, American Chemical Society.

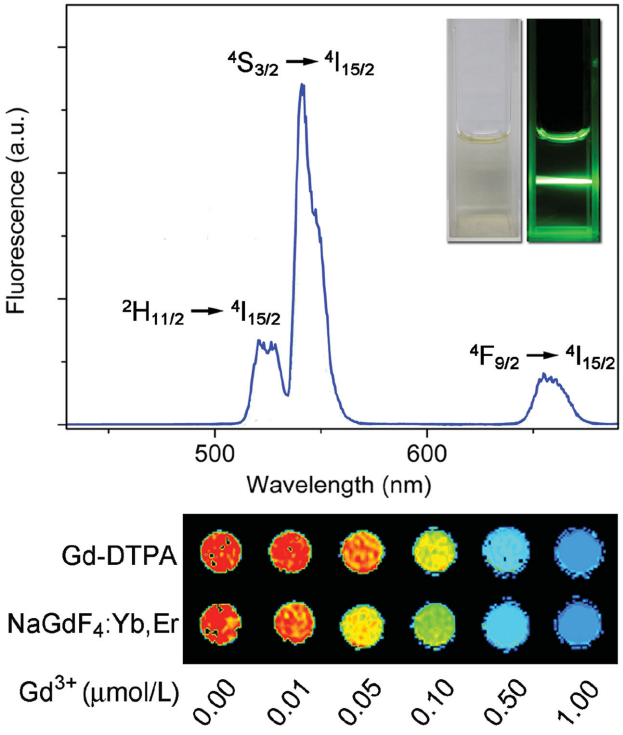

Figure 3. Upper panel: A typical luminescence spectrum of $NaGdF_4$:Yb,Er NPs recorded under excitation of CW 980 nm laser. The insets are photographs of a cyclohexane solution of NPs taken under ambient light (left) or in the dark under excitation by 980 nm laser (right); Lower panel: Color-coded T1-weighted MR images of aqueous solutions of the PEGylated $NaGdF_4$:Yb,Er NPs and Gd-DTPA with different Gd concentrations in 2 mL Eppendorf tubes. Adapted with permission.[18] Copyright 2013, American Chemical Society.

Shi and coworkers designed a core/shell NPs by seed-mediated growth technique, in which a 17.9 nm $NaYF_4$:Er,Yb,Gd particle was coated with a $NaYF_4$:Tm,Yb shell. The relaxivity measurements revealed that the shell of 4 nm was enough to decrease the relaxivity r_1 down to nearly zero. However, the relaxivity r_1 was recovered if the above core/shell particle was further coated with $NaGdF_4$, suggesting that Gd^{3+} ions on the particle surface or close to it dominate the T_1 enhancement effect of Gd-NPs, which is an important message for designing Gd-containing NPs for MRI applications.[45] Regarding the optical properties, Gao's group has demonstrated that coating $NaGdF_4$:Yb,Er core with $NaGdF_4$ shell could dramatically enhance the efficiency of the upconversion luminescence by near two orders of magnitude.[28]

Although the attractive properties of rare-earth (RE) NPs arouse great interests to explore their biomedical applications,[2] yet the toxicity concerns persist. The RE elements, especially lanthanides, are not actually found to naturally form part of any biological molecules. According to references, the non-radioactive lanthanides are less toxic than most other nondietary elements.[46] Further in vitro cellular studies suggested that RE^{3+} ions may interfere with Ca^{2+} channels owing to their comparable radius, thus affecting the physiological processes within the tissues.[47,48] Nevertheless, the rat studies suggested that Gd^{3+} is less toxic than Mn^{2+},[49] although the latter is also a useful paramagnetic ion for constructing T_1 contrast agents. Until now, most clinical MRI contrast agents are chosen from Gd-chelates due to their low release levels of free Gd^{3+} ions and quick renal clearance, although patients with renal disease are subjected to risks of severe complication such as nephrogenic systemic fibrosis.[50] A number of recent studies suggested that some inorganic matrices can also firmly hold Gd^{3+} showing very low release levels of free Gd^{3+} ions.[18,51] For example, the amount of free Gd^{3+} ions released by $NaGdF_4$ particles is calculated to be around 6 nmol mL^{-1}.[18] Based on rat experiments, the amount of $GdCl_3$ to kill 50% of the test animals (LD50) is about 0.5 mmol kg^{-1} body weight,[52] $NaGdF_4$ NPs are thus very likely innocuous. However, the toxicity of NPs in a broad sense is very complicated. It is associated not only with the release of metal ions, but also with the potential biological effects of nanomaterials. Numerous cytotoxicity tests based on cellular morphology and mitochondrial function suggested that RE NPs have low cytotoxicity to a broad range of cell lines under certain thresholds of particle concentration and incubation time.[18,44,53–59] The cytotoxicity tests of PEGylated $NaGdF_4$ (5.4 nm and 19.8 nm) and $NaGdF_4$:Yb,Er NPs (24.6 nm) on human gastric cancer cell line GC7901 revealed that the 80% cell viability was achieved for all particles at 10 mM Gd^{3+} (1.57 mg mL^{-1}) after 24 h incubation. The IC_{50} (50% inhibitory concentration) values were further determined to 16.5, 13.8, and 17.7 mmol L^{-1} for 5.4 nm $NaGdF_4$, 19.8 nm $NaGdF_4$, and 24.6 nm $NaGdF_4$:Yb,Er, respectively.[18,44] Long term (over 100 days) toxicity tests on RE NPs were previously carried out through weight fluctuation, histological, and biochemical analyses by Li and coworkers after RE NPs were intravenously injected into mice through tail vein and only small weight difference with reference to the control group was observed.[53] Further histological assessment of various tissues suggested that liver, kidney, and heart showed

no obvious changes except for spleen that was slightly hyperplasia. It was also demonstrated that the biodistribution and elimination pathways are strongly associated with particle size. For example, more than 87% of 18.5 nm PEGylated $NaGdF_4$:Yb,Er were excreted through the biliary eliminatin pathway 30 d postinjection and no difference in size, size distribution, and shape, if compared with the mother particle, was observed from the particles found in feces. In contrast, 5.1 nm PEGylated NPs were mainly excreted through renal clearance pathway, resulting in a much shorter biological half time in mice, i.e., 1.4 days vs 7.0 days for 18.5 nm NPs.[18] All above-mentioned studies can help to relieve the toxicity concerns on the potential biomedical applications of Gd-containing NPs.

2.2. Manganese-Based NPs

Different from Gd^{3+} ions, Mn^{2+} ions can directly be used as a contrast agent for pharmacological studies on the effects of drugs on neuronal activity, which is known as manganese-enhanced MRI (MEMRI).[60] It was also found out that no invasive procedures to breakdown the blood-brain barrier (BBB) is required to infuse $MnCl_2$ into brain parenchyma.[61] Once within the central nervous system, Mn^{2+} ions can quickly enter neurons through Ca^{2+} channels for the following MEMRI.[62] The optimal dose for MEMRI of rat visual pathway was previously found to be 150–300 nmol ivit $MnCl_2$.[60] Higher doses of Mn^{2+} ions are toxic. The acute toxicity is due to cardiovascular effects, while the chronic toxicity is due to cerebral or hepatobiliary damage.[63–65] To further suppress the toxicity of Mn^{2+},[66] Mn-chelates such as Mn-DPDP are developed as T_1 contrast agents.[67] Similar to the tendency of the development of Gd-based MRI contrast agents, from metal-complexes to NPs, manganese-based NPs have gained tremendous interests in the past a few years. Manganese has a number of valence states, but only in bivalent state it possesses five unpaired electron to produce efficient positive contrast enhancement.[68] The following stoichiometric inorganic manganese compounds such as MnO, Mn_3O_4, $KMnF_3$, etc., are found to be suitable for forming NPs with T_1 contrast enhancing effects. In addition, Mn^{2+} can be also used as a magnetic dopant of NPs for T_1 MR imaging.[69–71]

Regarding the synthesis of Mn-containing NPs, previous investigations suggest that wet-chemical synthetic routes are generally superior to physical synthetic methods with respect to morphological control over the resulting NPs. Among different wet-chemical synthetic routes, the thermal decomposition of Mn-organic compounds is largely adopted for achieving high-quality manganese oxide NPs.[72,73] In this synthetic route, oleylamine and oleic acid are often used as particle surface capping agents. Nevertheless, the different chemical properties of these two ligands lead to different forms of manganese oxides.[74] For example, pyrolyzing Mn (II) acetylacetonate[75,76] or $Mn(HCOO)_2$[77] in oleylamine gave rise to monodisperse Mn_3O_4 nanocrystals of 6–15 nm, while pyrolyzing manganese(II) acetate in trioctylamine in the presence of oleic acid led to monodisperse MnO nanocrystals of 7–20 nm.[78] Simply pyrolyzing Mn-oleate in oleic acid generated not only monodisperse spherical MnO nanocrystals but also monodisperse MnO nanocrystals with different sizes and shapes.[79–82] All these investigations suggest that even in an inert atmosphere, oleylamine is in favor of the formation of Mn_3O_4,[83] while oleic acid tends to give rise to MnO.[80,84] If oleylamine and oleic acid are used simultaneously as surface capping agents, the form of the resulting manganese oxide particles become quite dependent on the synthetic parameters. For example, octahedral MnO nanocrystals were obtained through the thermal decomposition of $Mn(Ac)_2$.[85] Both Mn_3O_4 and MnO nanocrystals were simultaneously formed upon the pyrolysis of $Mn(acac)_2$.[86] A recent study disclosed that the formation of Mn^{2+}-oleylamine is more kinetically favorable, while the formation of Mn^{2+}-oleate is more thermodynamically favorable. These differences lead to selective formation of manganese oxide NPs of different forms since Mn^{2+} in the form of Mn^{2+}-oleylamine is more prone to be oxidized than that in Mn^{2+}-oleate. Thus, the heating procedure plays a determining role in the selective synthesis of MnO and Mn_3O_4 nanocrystals by balancing the coordination of oleylamine/oleic acid to Mn^{2+}.[72] This new finding provides a flexible measure for tuning the chemical composition of manganese oxides NPs through the thermal decomposition approach, even though both MnO and Mn_3O_4 NPs show tremendous T_1 contrast enhancing effects after surface PEGylation.[74] Apart from the intrinsic magnetic properties of manganese, the longitudinal relaxivity is strongly correlated with the shape of manganese oxide NPs. Via different particle grow mechanisms, MnO dumbbells,[87] MnO nanoplates,[88] MnO multipods (MnO nanocrosses, MnO nanohexapods, MnO nanooctapods),[80,89] MnO nanoflowers,[90] and Mn_3O_4 nanokites[91] have been reported, which provides a rich set of morphologies for disclosing their impacts on T_1 contrast enhancement performance.

Regarding MRI applications of manganese oxide NPs as contrast agents, Hyeon and coworkers firstly reported the synthesis and relaxometric properties of uniformly sized MnO NPs of 7 nm, 15 nm, 20 nm, and 25 nm in 2007. The MnO NPs were synthesized through the thermal decomposition of Mn-oleate complex and the particle size was effectively tuned by varying either reaction time or solvent. With PEG (polyethylene glycol)-phospholipid the as-prepared hydrophobic NPs were transferred into aqueous media and exhibited a clear particle size-dependent r_1 ranging from 0.37 mM^{-1} s^{-1} for 7 nm NPs to 0.12 mM^{-1} s^{-1} for 25 nm NPs.[92] Latter studies revealed that the PEG-phospholipid-coated MnO NPs were prone to be oxidized from the surface to form a Mn_3O_4 shell structure. By selectively dissolving the MnO core, the remaining Mn_3O_4 hollow particles presented a r_1 value (1.42 mM^{-1} s^{-1} measured at 3 T) higher than that (0.21 mM^{-1} s^{-1}) for solid MnO NPs, which was attributed to the increased amount of Mn^{2+} exposed at the inner surface of the hollow particles. In the meantime, the latter structure also exhibited T_2 effect which may originate from the transformation from MnO to Mn_3O_4.[93]

Different from the solid/hollow manganese NPs, PEGylated MnO nanoplates, prepared through the pyrolysis

of manganese(II) acetylacetonate in the presence of 2,3-dihydroxynaphthalene and then coated with PEG through a ligand exchange process, presented much higher longitudinal relaxivity. The r_1 value of MnO nanoplates of 1 nm × 8 nm was determined to be around 5.5 $mM^{-1}s^{-1}$ at 1.5 T,[88] higher than those for MnO spherical NPs and MnO hollow NPs due to largest surface-to-volume ratio for ultra-thin nanosheet structure.

PEG-coated $KMnF_3$ NPs of 20 nm were recently reported as a new type of manganese based T_1-weighted contrast agent. The NPs were synthesized through a solvothermal process via the reaction between potassium fluoride dehydrate ($KF{\cdot}2H_2O$) and manganese chloride tetrahydrate ($MnCl_2{\cdot}4H_2O$) in presence of potassium oleate in a mixture of ethanol and hexane. After PEG coating, the longitudinal relaxivity r_1 and transverse relaxivity r_2 were determined at 3 T to be 23.15 mM^{-1} s^{-1} and 74.85 mM^{-1} s^{-1}, respectively.[94] The high relativity values of $KMnF_3$ NPs were attributed to the exposure of surface Mn^{2+} ions, yet in-depth studies remain in the lack for understanding the extraordinary T_1/T_2 performance, at least to exclude the potential effects of particle aggregation on the T_1/T_2 performance.

Manganese oxides occur in different forms, not all of them are suitable for preparing T_1 contrast agents. For example, MnO_2 nanosheets showed neglectable MRI contrast enhancing effect. However, MnO_2 is prone to be reduced to release Mn^{2+}. They therefore were used for developing an activatable fluorescence/MRI bifunctional imaging probes.[95]

The unique magnetic property also allows Mn^{2+} ions as a dopant for achieving multifunctional NPs.[71,96] For example, Gao and coworkers synthesized highly fluorescent CdTe@ZnS core/shell structured quantum dots (QDs).[70] By doping the ZnS shell with Mn^{2+}, aqueous QDs with strong fluorescence and high relaxivity were obtained. They further employed the same strategy to achieve Cd-free $CuInS_2$@ZnS:Mn QDs that not only presented excellent optical imaging and MR imaging potentials, but also extremely low cytotoxicity in comparison with CdTe QDs.[69]

2.3. Iron-Based NPs

Unlike gadolinium, iron is one of the most abundant metallic elements in living organisms and essential for various biological processes, including oxygen transport by hemoglobin and cellular respiration by redox enzymes. Iron oxide NPs are known to be biologically well tolerated and benign. In addition to their superior biocompatibility, the superparamagnetism makes the magnetite and maghemite NPs exhibit strong T_2 effects thus offering much higher sensitivity than gadolinium complexes as for MRI.[97] Thus far, several iron oxide NPs have been approved for clinical use such as Feridex and Fereheme. Our previous review articles have comprehensively summarized the syntheses of magnetic iron oxide NPs towards biomedical applications.[12,98] In this review, we are focusing on the recent progress in iron oxide NP-based MRI contrast agents and imaging probes reported over the last 5 years.

Non-hydrolytic synthetic routes, especially the synthetic route based on the pyrolysis of various Fe organometallic compounds remain dominant for producing high quality iron oxide NPs. In 1999, Alivisatos group firstly reported uniform γ-Fe_2O_3 nanocrystals obtained by pyrolyzing $FeCup_3$ (Cup: *N*-nitrosophenylhydroxylamine, $C_6H_5N(NO)O^-$) in trioctylamine at temperature above 200°C by using octylamine as the particle surface capping agent.[99] Since then, the thermal decomposition method was quickly developed by Hyeon,[100] Sun,[101] Peng,[102] etc. for producing monodisperse magnetic iron oxide NPs of different sizes, shape, and even in gram scale.[79]

However, the direct NP products of thermal decomposition approach as mentioned above are typically hydrophobic since oleic acid and/or olylamine are widely used as particle surface capping agents. Therefore, they cannot directly be used for MRI applications. Towards MRI applications, Gao's group further developed the thermal decomposition method with the main results being summarized in **Figure 4**. By using strong polar high boiling point 2-pyrrolidone instead of the non-polar solvent, through the pyrolysis of $Fe(acac)_3$,

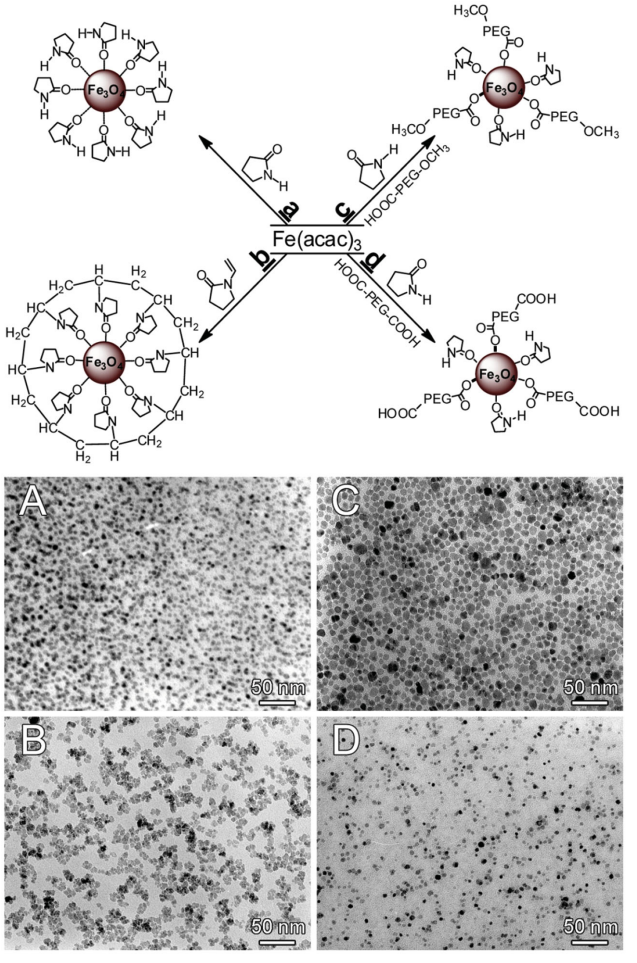

Figure 4. A summary of 2-pyrrolidone-based synthetic routes for producing high quality Fe_3O_4 with difference surface structures together with representative TEM images obtained through the corresponding routes. Adapted with permission for A[103] and B,[105] Copyright 2004 and 2008, American Chemical Society; C,[107] Copyright 2005, Wiley-VCH; D,[109] Copyright 2006, Wiley-VCH.

differently sized Fe_3O_4 NPs dispersible in aqueous media in acidic or alkaline ranges can be obtained.[103] Owing to coordination of the carbonyl group of 2-pyrrolidone to Fe^{3+}, no additional surface capping agent is required in this synthetic route to achieve nanometer sized Fe_3O_4 NPs. In-depth mechanism studies further reveal that the slow thermal decomposition of 2-pyrrolidone plays a key role in the formation of Fe_3O_4 as the slowly released of CO partially converts Fe^{3+} to Fe^{2+}.[104] Based on similar strategy, by using *N*-vinyl-2-pyrolidone instead of 2-pyrrolidone, the same synthetic route allows to produce super-dispersible Fe_3O_4 NPs in consequence of the in situ polymerization of the surface capping agent, i.e., *N*-vinyl-2-pyrolidone. The resulting poly(*N*-vinyl-2-pyrolidone) (PVP) coated Fe_3O_4 NPs can well be dissolved in neutral water, and phosphate buffered saline buffer apart from 10 different types of organic solvents to form colloidally stable solutions.[105] The same method can also be used to prepare PVP-coated $Ni_{0.6}Fe_{2.4}O_2$ NPs.[106] The excellent solubility of PEG in 2-pyrrolidone further allows the preparation of PEGylated Fe_3O_4 NPs through the pyrolysis of $Fe(acac)_3$ in the presence of a carboxylated PEG2000 ligand,[107] thus opening up a novel way for directly synthesizing high quality biocompatible Fe_3O_4 NPs for biomedical applications. In addition, by using α,ω-dicarboxyl-terminated PEG as surface capping molecule instead of monocarboxyl-terminated PEG, magnetic NPs with surface reactive moieties can be obtained.[108–110]

The following studies of the same group reveal that some 2-pyrrolidone molecules remain anchoring on the surface of Fe_3O_4 NPs prepared even in the presence of carboxylated PEG, which leads to the positive surface potentials for the PEGylated Fe_3O_4 NPs and thus becomes unfavorable for reducing the adsorption of plasma proteins. Owing to the excellent solubility of PEG in diphenyl oxide, a common less polar high boiling point solvent, the pyrolysis of $Fe(acac)_3$ enables the preparation of PEGylated Fe_3O_4 in the presence of oleylamine and carboxylated PEG. Different from the Fe_3O_4 NPs co-stabilized by 2-pyrrolidone and PEG, the latter Fe_3O_4 NPs are co-stabilized by oleylamine and PEG. The different surface chemical modifications for Fe_3O_4 NPs with comparable size and organic contents give rise to different behaviors when the NPs meet with highly abundant plasma proteins such as serum albumin and immunoglobulin G.[111]

Until now, most iron oxide NPs reported in literatures are prepared through batch preparations. To achieve large scale production, the reproducibility of batch preparations remains problematic. Not until recently, Gao's group reported a flow synthesis of the PEGylated Fe_3O_4 NPs with steady quality, as shown in **Figure 5**. Careful investigations revealed that lowering the linear velocity of laminar flow narrows the particle size distribution due to effectively suppressed residence time distribution, but the simultaneously prolonged residence time encourages Ostwald ripening leading to a reverse tendency for particle size distribution. Moreover, the monomer concentration distribution within the tube reactor, strongly associated with the flow parameters, i.e., linear velocity of the reaction flow and tube reactor diameter, largely affects the particle size distribution. Under the guidance of these findings, PEGylated Fe_3O_4 NPs with size distribution sufficiently narrower than that achieved through batch preparation were obtained. Moreover, the resulting particles (4.6 nm) exhibited excellent colloidal stability and high longitudinal relaxivity up to 11.1 mM^{-1} s^{-1}, which manifested the reliability of flow synthesis for preparing PEGylated Fe_3O_4 NPs as contrast agents for MRI applications.[21]

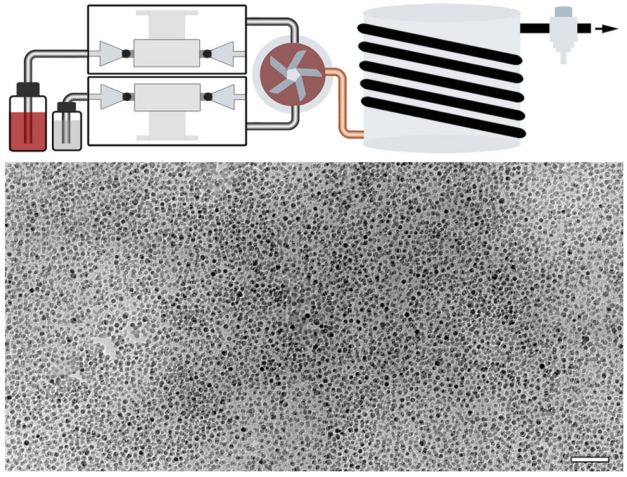

Figure 5. Sketch of the flow synthesis system and a representative TEM image of the PEGylated Fe_3O_4 NPs prepared under optimized conditions with the flow synthesis system. The scale bars correspond to 50 nm. Adapted with permission.[21] Copyright 2015, American Chemical Society.

It was further observed that the coordination between the particle surface capping agent and the metal precursor has strong impacts on the particle growth kinetics. For example, in a typical reaction system comprising of $Fe(acac)_3$ (precusor), HOOC-PEG-COOH/oleylamine (surface capping agent), and diphenyl (solvent), for synthesizing the PEGylated Fe_3O_4 NPs, $Fe(acac)_3$ can spontaneously form large molecular networks with the PEG ligand HOOC-PEG-COOH with the help of oleylamine before they break down to form Fe_3O_4 NPs. The formation of the molecular networks can be accelerated by temperature and time, which reduces the thermal decomposition rate constants of the Fe precursors in the new forms. Consequently the size of biocompatible Fe_3O_4 NPs can largely be tuned by altering the growth kinetics through the gelification of the reaction systems with no need to vary the preparation recipe.[112] More detailed results are summarized in **Figure 6**. In fact, the strong coordination between the surface capping agents and metal ions is ubiquitous for synthesizing colloidal particles. This interaction often results in supramolecular structures especially in organic system, which provides a new approach not only for tuning the particle size but also for obtaining NPs with unique morphologies.[113]

Apart from the gelification effects, air-bubbles present in the reaction system are also found to be effective for manipulating the particle growth kinetics. Cao and coworkers reported an interesting mechanism study of the bubbling effects on the monodispersity of the resulting iron oxide NPs prepared by pyrolizing iron oleate in 1-octadecence.[114] They demonstrated that the gas bubbles from either the boiling solvent or the inert atmosphere introduced largely

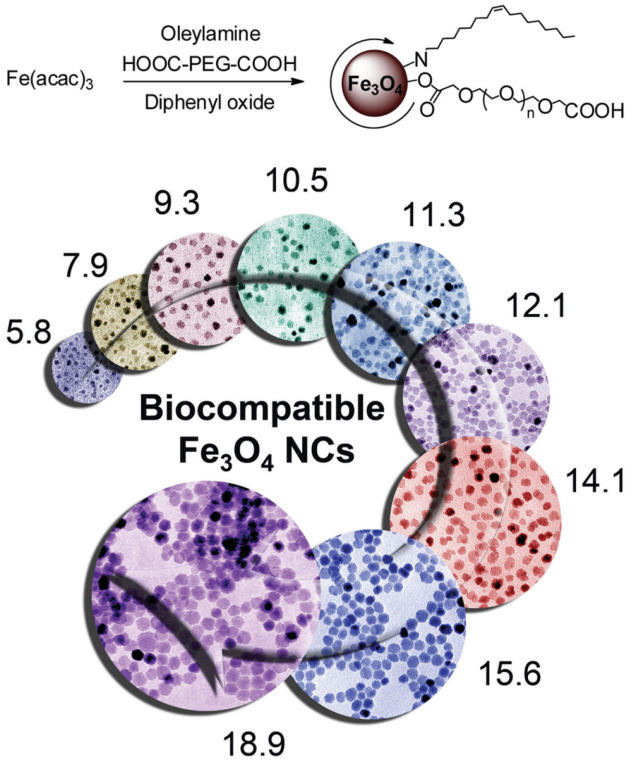

Figure 6. Upper panel: the synthetic route for synthesizing PEGylated Fe_3O_4 NPs through one-pot reaction; Lower panel: effective particle size regulation achieved by tuning the reaction time (5.8–11.3 nm) or viscosity of the stock solution through aging at different temperatures for different periods of time (12.1–18.9 nm). Adapted with permission.[112] Copyright 2011, American Chemical Society.

affect dissipation of local heat from the exothermic reactions involved in the nucleation and growth of iron oxide nanocrystals. Thus, the nucleation and the following growth processes can well be separated so as to achieve monodisperse iron oxide nanocrystals.

Theoretically, the relaxometric properties of iron oxide NPs are strongly associated with the particle size. Hyeon and coworkers reported the highest r_2 relaxivity up to 761 mM^{-1} s^{-1} (measured at 3 T) of 22 nm PEG-phospholipid-encapsulated iron oxide nanocubes, which was explained by the fact that the particle size falls in the static dephasing regime where the highest r_2 is expected according to theory.[115]

Apart from particle size, particle morphology also plays an important role determining the relaxometric properties of iron oxide NPs. It was recently observed that the faceted iron oxide NPs presented superior magnetism and relaxivities to the spherical counterparts.[116] Gao and coworkers further reported octapod-shaped iron oxide NPs exhibiting ultrahigh r_2 relaxivity up to 679.3 mM^{-1} s^{-1} measured at 7 T, contrasting to 125.7 mM^{-1} s^{-1} for spherical iron oxide NPs with a similar effective diameter. The authors attributed the extremely high r_2 to a more inhomogeneous local magnetic field induced by the octapod structure.[117]

The iron oxide NPs have largely been used as T_2 contrast agents due to the unique superparamagnetic properties. However, the paramagnetism becomes dominant as the size of iron oxide nanoparticle decreases due to the increased degree of spin disorder on the particle surface.[118] In consequence, the small iron oxide NPs becomes a potential candidate for T_1 contrast agents. The additional benefit of small particles is their quick renal clearance.[18]

By the thermal decomposition method, Sun and coworkers reported very small Fe_3O_4 NPs prepared upon the pyrolysis of $Fe(acac)_3$ in phenyl ether in the presence of alcohol, oleic acid, and oleylamine.[101] Based on this method, Weller and coworkers synthesized 4 and 6 nm hydrophobic iron oxide NPs and then transferred them into aqueous solution using phosphate-functionalized PEG with different chain lengths.[119] The following studies suggested that the Fe_3O_4 NPs stabilized by PEG350 tended to aggregate, while those stabilized by PEG550, PEG1100 and PEG2000, respectively, were more colloidally stable. Under comparable conditions, 6 nm iron oxide NPs presented higher r_1 and r_2 values than 4 nm NPs at 1.41 T, due to higher saturation magnetization of the larger nanocrystals. Under optimized conditions, 4 nm NPs capped by PEG1100 presented a r_1 relaxivity of 7.3 mM^{-1} s^{-1} higher than that of Gd-DTPA and a low r_2/r_1 ratio of 2.4 as well.

The thermal decomposition of iron-oleate complex in diphenyl ether containing oleyl alcohol and oleic acid also provided the possibility of large scale synthesis of monodisperse iron oxide NPs smaller than 4 nm.[22] Upon ligand exchange with PEG-derivatized phosphine oxide (PO) ligand, the resulting particles of 3 nm exhibited r_1 relaxivity of 4.78 mM^{-1} s^{-1} and r_2/r_1 ratio of 6.12 at 3 T. In contrast, 5.4 nm PEGylated Fe_3O_4 NPs prepared through the facile one-pot synthetic route developed by Gao and coworkers presented very high r_1 of 19.7 mM^{-1} s^{-1} (at 1.5 T) and low r_2/r_1 ratio of 2.0.[120]

In literature, great efforts have been spent to suppress the r_2/r_1 ratio down to at least 5 in order to enable the application of small iron oxide particles as T_1 contrast agents, but mainly through size reduction.[17,27,119–122] Nevertheless, a recent study by Gao and coworkers suggests that this criterion for judging the suitability of iron oxide NPs may need to be reconsidered. In their study, they firstly synthesized two differently sized Fe_3O_4 NPs, i.e., 3.6 nm and 10.9 nm. By replacing the hydrophobilic ligands with PEG2000 ligand bearing diphosphate (DP), hydroxamate (HX), and catechol (CC) groups, respectively, PEGylated Fe_3O_4 NPs were obtained. Further relaxometric measurements revealed that CC-PEG and HX-PEG capped particles presented stronger T_2 and T_1 effects than those capped by DP-PEG, which became significant for Fe_3O_4 particles of 3.6 nm as shown in **Figure 7**. Moreover, HX-PEG and CC-PEG modifications also gave rise to higher r_2/r_1 ratio due to the enhanced r_2, which was explained by the positive contribution of π–π and p–π conjugation structure of the anchoring group of the PEG ligand to the inhomogeneity of the local magnetic field around the underlying Fe_3O_4 NPs. Although the r_2/r_1 ratio was as high as 11.6, the 3.6 nm Fe_3O_4 NPs capped by HX-PEG presented effective contrast enhancement effects for both T_1 and T_2 imaging (Figure 7). Most importantly, the above studies for the first time clearly disclosed the impacts of the anchoring group of the nondisposable particle surface ligand on the relaxometric properties of the underlying

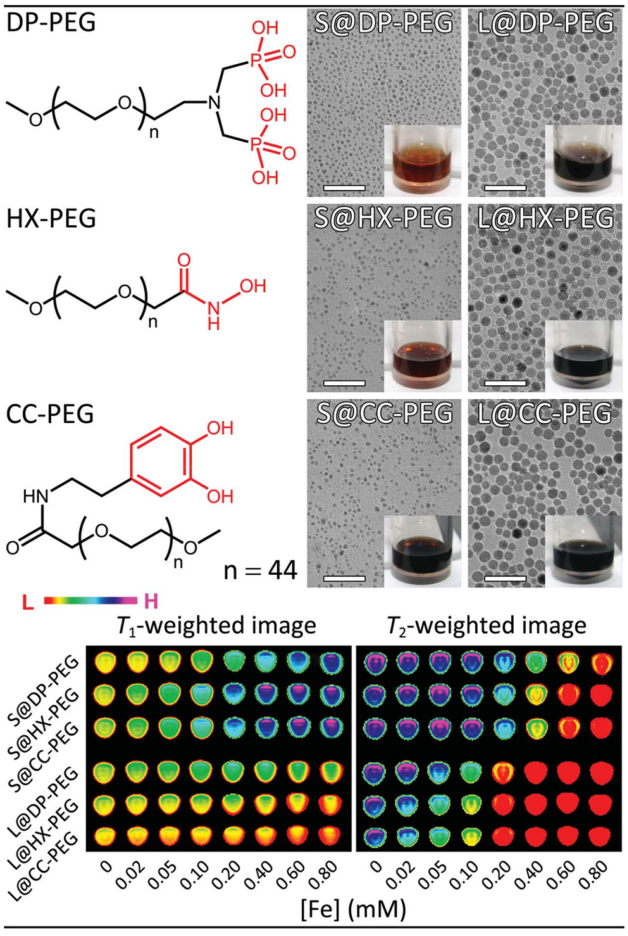

Figure 7. Upper panel: chemical structures of three PEG ligands bearing different anchoring groups for exchanging the hydrophobic ligands of 3.6 nm Fe_3O_4 NPs (S) and 10.9 nm Fe_3O_4 NPs (L), together with TEM images of the resulting PEGylated particles. The embedded scale bars correspond to 50 nm and insets are photographs of aqueous solutions of the PEGylated Fe_3O_4 particles with an equal Fe concentration of 20 mM. Lower panel: T_1-weighted and T_2-weighted MR images of aqueous solutions containing 3.6 nm or 10.9 nm Fe_3O_4 NPs capped by different PEG ligands, respectively. Adapted with permission.[17] Copyright 2014, Wiley-VCH.

magnetic NPs, which provides a novel strategy for tailoring the relaxometric properties of magnetic NPs for versatile biomedical applications.[17]

Apart from iron oxides, iron carbides are potential candidates as well for producing nanoparticulate contrast agents due to their rather high saturation magnetization.[123,124] Recently, a facile one-pot wet-chemistry route for preparing iron carbide (Fe_5C_2) NPs was reported, in which $Fe(CO)_5$ was used as iron precursor and octadecylamine served as a coordinating solvent. Upon reaction at 350°C Fe_5C_2 nanocrystals with an average size of 20 nm were obtained with the help of cetyltrimethylammonium bromide.[125] Through surface modification using 1,2-distearoyl-*sn*-glycero-3-phosphoethanolamine-*N*-[amino(polyethylene glycol)-2000], the transverse relaxivity r_2 of the resulting NPs was determined to be 312 $mM^{-1}\cdot s^{-1}$ at 3 T,[126] higher than that of iron oxide NPs of similar sizes.[127]

3. Surface Modifications

In general, the non-aqueous synthetic routes represented by the thermal decomposition method offer a nice approach for precisely control the size of magnetic NPs. Although Gao and coworkers have paved a facile way based the thermal decomposition method for directly synthesizing monodisperse Fe_3O_4 NPs with biocompatible surface, mostly the NPs obtained are hydrophobic due to use of surface capping agents bearing long alkyl chain molecules. Therefore, adequate surface modifications are essentially required to enable the NPs water soluble, biocompatible, surface functionalizable for biomedical applications. In general, the following approaches have been developed towards these needs, e.g., amphiphilic molecule encapsulation, inorganic encapsulation, ligand oxidation, and surface ligand exchange.

Among them, amphiphilic molecule encapsulation is achieved mainly based on the hydrophobic-hydrophobic interactions between the hydrophobic particle surface ligand and the hydrophobic segments of amphiphilic molecules such as poly(maleic anhydride) derivatives,[128] PEG-derivatized phosphine oxide, PEG-phospholipid, or dual-interaction including both hydrophobic-hydrophobic interaction and coordinating interaction of Tween derivatives,[129,130] or multiple-interaction interactions for a copolymer composed of PEG, polyethylenimine, and poly(L-3,4-dihydroxyphenylalanine), etc. Nevertheless, all these surface encapsulation approaches leave a hydrophobic layer behind, which may be unfavorable for contrast enhancement effects due to the poor access of water molecules to the surface of magnetic NPs. Yet the amphiphilic molecule encapsulation approaches are generally very effective for transferring hydrophobic NPs to aqueous media, regardless of the chemical composition of the particle cores.

Apart from the amphiphilic molecule encapsulation, coating the hydrophobic NPs with inorganic materials were adopted for introducing additional functions to the magnetic particles. For example, the TaO_x shell of Fe_3O_4@TaO_x core/shell particles prepared in reverse micelles could enhance the contrast of X-ray computer tomography (CT),[131] the same idea was also used by coating iron oxide nanoparticle with Au shell or forming Fe-Au alloy.[132,133] Owing to the porous structure, magnetic NPs coated with silica shell for loading drugs were also reported for tumor theranostics.[134]

As aforementioned, oleic acid is almost the most suitable surface capping agent for versatile magnetic NPs prepared via the thermal decomposition methods. To convert the resulting hydrophobic NPs into hydrophilic ones, oxidization reactions with Lemieus-von Rudloff reagent were reported to convert the oleic acid into azelaic acid to render the underlying particles water solubility.[135,136] Nevertheless, this approach largely changed the particle size distribution probably due to the etching effect of the reagents.

Alternatively, the hydrophobic NPs can be converted into hydrophilic ones upon post ligand exchange process. Determined by the binding affinity of the anchoring group of water soluble ligand to metal ions of the NPs, versatile water soluble and biocompatible ligands with anchoring groups such as (di)phosphate, hydroxamate,

catechol, multi-thiols, multi-carboxyl, have been synthesized and adopted for replacing the hydrophobic ligands of the magnetic NPs.[17,18,44,129,137,138] Although surface ligand exchange often leads to different degrees of particle agglomeration in aqueous media, it remains a reliable approach upon proper design of the water soluble ligands. For example, the oleate ligands of Fe_3O_4 NPs can be replaced by DP-PEG2000, HX-PEG2000, and CC-PEG2000 ligands, respectively, without altering the hydrodynamic size profiles of the water-soluble particles.[17] This approach is also applicable for replacing the oleate ligand of $NaGdF_4$ NPs with DP-PEG2000. If the DP-PEG2000 ligand bears a reactive maleimide group at the other end, the asymmetric PEG also facilitates the following bio-conjugation of the underlying NPs with biotargeting molecules such as antibody through an efficient click-reaction taking place under mild conditions.[18,28,44] With respect to biomedical applications, anti-biofouling properties of the surface coating are essential for efficiently directing the NPs to the region of interest. Although PEGs with suitable molecular weights have been considered as outstanding anti-biofouling materials, zwitterion was also found to have superior anti-biofouling properties. Also through surface ligand exchange process, Bawendi and coworkers reported compact zwitterion-coated iron oxide NPs with excellent colloidal stability in a pH range of 6.0–8.5. Most importantly, the zwitterion-coating contributed to the hydrodynamic size of the NPs much less than PEG and dextran that are often used as anti-biofouling materials for coating magnetic NPs.[139] In fact, the syntheses of water-soluble zwitterionic ligands are complicated. However, through ligand exchange with sodium 10-mercaptodecanesulfonic acid and (10-mercaptodecyl)-trimethyl-ammonium bromide, NPs with zwitterionic surface can be obtained, which opens up a flexible approach towards the surface modifications of magnetic NPs for biomedical applications.[140]

So far, most ligand exchange approaches rely on a stronger binding affinity of the new ligands. Dong et al. recently developed a novel ligand-exchange strategy which could overcome this limit.[141] It has be confirmed that nitrosonium tetrafluoroborate ($NOBF_4$) can effectively replace the hydrophobic ligands including oleic acid and oleylamine, independent of the particle core composition and shape. Since NO^+ is readily being reduced, leaving BF_4^- attached onto the nanocrystal surface. The resulting BF_4^--capped nanocrystals can well be dispersed in various polar and hydrophilic media such as *N*,*N*-dmethylformamide, dimethylsulfoxide, or acetonitrile. However, BF_4^- does not have a strong binding affinity to nanocrystal surface, which allows the re-attachment of new ligands to achieve ligand replacement. This interesting approach should be very valuable for functionalizing the magnetic NPs with designed surface structures.

4. Applications

4.1. Blood Pool Imaging

A prerequisite ensuring efficient blood pool imaging is long enough blood circulation time for contrast agents. However, the commercial MRI contrast agents, i.e., gadolinium complexes, are rapidly excreted through the kidney/urine, showing very short blood half-times. For example, Gd-DOTA only exhibits a time window of around 10 min for enhancing the contrast of blood pool, which hampers the high-resolution imaging which requires long scanning time.

In contrast, due to much larger dimensions, NPs could present longer intravascular half-life upon suitable surface modification. But the particle size is one of major parameters to balance the renal clearance and the reticuloendothelial uptake that are strongly associated with the blood residence time of NPs. Hyeon's group reported extremely small (< 4 nm) and uniform iron oxide NPs capped with PO-PEG ligands as T_1 contrast agents.[22] After the intravenous injection, the blood vessels were strongly brightened on the T_1-weighted MR images for 1 h. In consequence, time-consuming 3d-FLASH sequence was enabled to achieve high-resolution T_1 imaging of blood vessels with a diameter down to 0.2 mm.

4.2. Atherosclerosis Imaging

The sudden rupture of the atherosclerotic plaques induces acute thrombotic occlusion of the artery and myocardial infarction or stroke. These catastrophic events are difficult to predict solely with anatomic information, because the plaque vulnerability is strongly linked to plaque composition but not necessarily to the degree of luminal narrowing. Indeed, many infarcts originate from non-obstructive vulnerable plaques.

Noninvasively detecting the plaque components particularly those mediating the transition of stable plaques to vulnerable/high-risk plaques remains challenging but very important for monitoring and predicting the cardiovascular events. Oxidized low-density lipoprotein (OxLDL) is a heterogeneous entity that contains a variety of oxidation-specific epitopes that mediate immunological and inflammatory pathways leading to atherogenesis. OxLDL has been identified as a key factor in the initiation, progression, and destabilization of vulnerable atherosclerotic plaques in both animals and humans, and thus can potentially used as a target for imaging rupture prone plaques. Recently, an OxLDL-targeting magnetic NP probe was prepared, by conjugating the anti-mouse OxLDL polyclonal antibody to iron oxide NPs capped by HOOC-PEG-COOH through the carboxylic groups, for imaging atherosclerotic lesions in a carotid perivascular collar model based on apolipoprotein E-deficient mice. The resulting OxLDL-specific probe gave rise to T_2-weighted MR signal loss up to 30–35% after intravenous administration. In huge contrast, signal loss around 4–5% was observed from a control probe formed by the same NPs with irrelevant IgG. Further immunohistochemical studies confirmed the co-localization of the OxLDL/macrophages and iron oxide NPs, suggesting that the above probe could detect OxLDL and atherosclerotic lesion via enhanced MRI.[142] In a similar way, the same group also reported an alternative MR imaging probe based on lectin-like oxidized low-density lipoprotein receptor 1 (LOX-1).[143] Apart from detecting carotid atherosclerotic lesions, the resulting probe also showed potentials

in detecting kidney inflammation owing to the expression of LOX-1 in the kidney glomerulus of apoE$^{-/-}$ mice.

Macrophages rupture atherosclerotic plaques by digesting extracellular matrix. For that reason, macrophage imaging with magnetic NPs is highly attractive and may potentially be used for identifying high-risk vascular regions, predicting the risk of plaque rupture, and evaluating the therapies.[144–147] Clinical imaging of plaque macrophages is still challenging, because the volume of interest in coronaries and carotids is small. In addition, specific labeling of atherosclerotic plaque-associated macrophages with nanoprobes remains in lack.

4.3. Cell Imaging

Owing to the great potential of cell-based treatment, tracking cells in vivo arises increasing interests. MRI is superior in assessing the location and migration of labeled cells due to its high spatial resolution with respect to imaging. In this context, magnetic NPs as contrast agents provide an excellent platform due to the high cellular uptake efficacy upon suitable surface design apart from their high relaxivity. Iron oxide NPs are probably the most extensively explored contrast agents for labeling cells such as mesenchymal stem cells (MSCs),[148] neural stem cells,[149] dendritic cells,[150] etc. It was found out that the adsorption of human serum albumin on dopamine-coated iron oxide NPs could effectively facilitate the cellular uptake of iron oxide NPs by various types of cells.[151] Due to the hypointensive signal of conventional iron oxide particle-labeled cells, hypointense regions such hemorrhage and blood clots may cause signal interference in vivo. Paramagnetic NPs therefore become an alternative choice. Hyeon's Group reported a novel design of MnO NPs that possess a 'hollow' MnO core and a mesoporous silica shell. The negative surface potential of the MnO NPs allowed effective cell labeling through electroporation. In vivo experiments revealed that a hyperintense signal from the site transplanted with labeled MSCs lasted for over 14 days.[152]

4.4. Cancer Imaging

Cancer, a group of diseases involving abnormal cell growth with the potential to invade or spread to other parts of the body, remains one of the world's most devastating diseases.[153] Early detection of cancers is believed to be the key step for successful cancer therapy but remains tremendously challenging.[154] MRI represents one of the most effective noninvasive techniques for cancer detection. However, the MRI contrast between biological background and cancerous tissue is not sufficient enough for achieving early detection.

Owing to the excellent contrast enhancement ability, magnetic NPs are widely studied as contrast agents for early tumor detections. One of the most important reasons is that the vasculatures of tumors are disordered and leaky, giving rise to enhanced permeability for NPs, while the poor lymphatic drainage in tumors encourages the retention of nanometer-size particles, which is widely known as tumor-associated EPR effect.[15] The additional advantages of using NPs for tumor imaging include: 1) upon proper surface modification, the underlying NPs can present prolonged blood half-time that is favorable for enhancing the accumulation of NPs within tumors;[111] 2) the multiple surface binding sites of NPs allow the integration of different functional units not only for increasing the tumor binding specificity but also for multimodality imaging,[16,155,156] but reliable surface functionalization chemistry is essentially required;[18,44,109] 3) magnetic NPs can not only provide imaging function but also act as a carrier to achieve activable probes for revealing the malignance of tumor microenvironment;[16] 4) magnetic NPs can also perform as a nanocarrier for achieving theranostic probes,[157] which adds additional values with respect to translational medicine.

Gao and coworkers reported a T_1/T_2 dual-modality MR imaging agent based on the intrinsic relaxometric properties of 3.6 nm HX-PEG-coated Fe_3O_4 NPs and tremendously high ΔR_1 and ΔR_2 up to 33% and of 54%, respectively, were achieved through EPR effect for imaging the same tumor site after intravenous injection of the dual-modality contrast agent. The detailed results are shown in **Figure 8**.[17] Also through EPR, an interesting tumor microenvironment

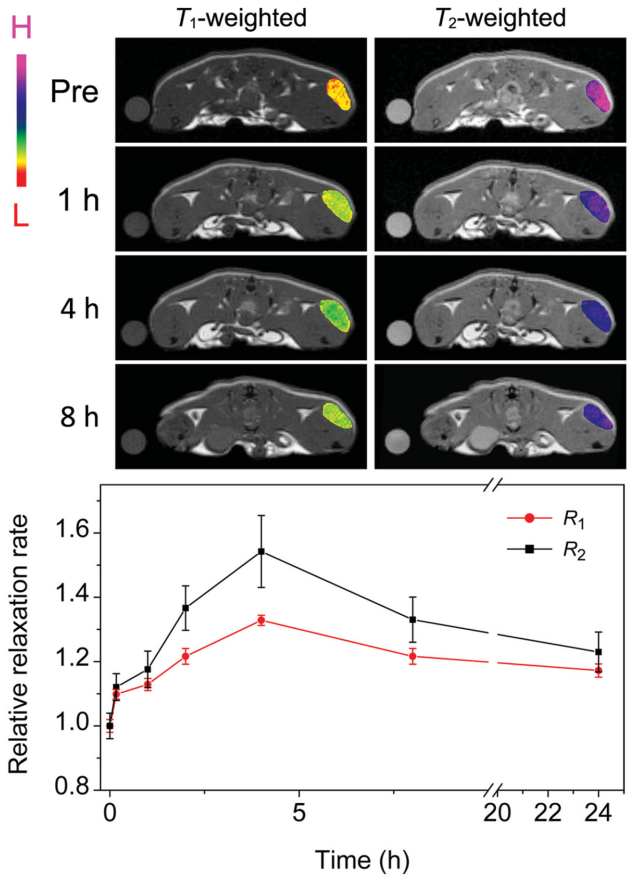

Figure 8. Upper panel: T_1-weighted and T_2-weighted MR images of nude mouse bearing a subcutaneously transplanted tumor acquired before (Pre) and at 1, 4, and 8 h postinjection of HX-PEG coated 3.6 nm Fe_3O_4 NPs through tail vein, the tumor site is color-coded for better showing the T_1/T_2 contrast enhancement effects; Lower panel: relative R_1 and R_2 values of the tumor site extracted at different time points postinjection. Reproduced with permission.[17] Copyright 2014 Wiley-VCH.

triggering drug delivery was reported by Grimm and coworkers recently.[157] Normally, the tumor microenvironment is characterized by abnormal extracellular pH typically in a range of 6.2–6.9 slightly lower than that (7.2–7.4) for normal tissues in consequence of anaerobic glycolysis. Based on this slight pH discrepancy, they prepared a drug releasing system by using commercial iron oxide NPs (Ferumoxytol) as a carrier to load tumor drugs such as Doxorubicin through the weak electrostatic interactions between the drugs and the dextran coating of iron oxide NPs. The cargo-loaded Ferumoxytol presented good serum stability over days and the loaded drug could be released below pH 6.8. Further therapeutic studies on nude male mice bearing PC3-derived prostate cancer xenografts and nude female mice with breast cancer BT20 tumors revealed that the drug-loaded NPs were considerably more effective than the free drugs, following intravenous administration. They also found that as the drug content in the NPs increased, the T_1 and T_2 relaxation times rose also over those of the unloaded NPs, which provided an option for noninvasively monitoring the drug delivery in vivo.

With respect to noninvasive tumor diagnosis, the remarkable challenges include early tumor detections, tumor metastasis visualization, and tumor microenvironment detection apart from overcoming various biological barriers. To meet these challenges, bioligand-guided active targeting strategy is believed to be superior to passive tumor targeting through EPR effect.

In fact, early tumor diagnosis through imaging techniques is to challenge the bottom visualizable size of tumors. To this purpose, the imaging properties of NPs have to be maximized. Moreover, suitable particle surface modification and proper tumor-specific bioligands are essentially optimized for better holding the NPs within tumors. Through anti-epidermal growth factor receptor monoclonal antibody (mAb), Gao's group reported a series of paramagnetic NP-based tumor-specific probes for realizing tiny tumor imaging. They designed an asymmetric PEG ligand bearing both biphosphate group and maleimide group. Since the biphosphate group possesses higher binding affinity to rare-earth element, the asymmetric ligand was used to replace the original hydrophobic oleate ligand to render the $NaGdF_4$ NPs biocompatibility, while the maleimide was used to covalently conjugate monoclonal antibody to the particle surface through highly efficient click reaction between PEG ligand and mAb bearing thiol groups.[44] The rationally designed probes presented excellent tumor binding specificity in detecting intraperitoneal tumor xenografts in nude mice through MRI with ΔT_1 of tumor sites climbing up to 30–50%. Based on these successful results, they further reported a similarly structured tumor probe with paramagnetic/upconversion luminescent $NaGdF_4$:Yb,Er NPs for dual-modality imaging of tumor xenografts.[18] The resulting probes were not only used to image subcutaneous and intraperitoneal tumor xenografts through MRI (upper frame of **Figure 9**), but also used to image the tumors through upconversion luminescence. Owing to the excellent properties of the dual-modality imaging probes, subcutaneous tumors as small as 1.7 mm × 1.9 mm were optically located in vivo (lower frame of Figure 9).

Lymphatic system offers one of the easiest paths for malignant cancer cells to spread while regional lymph nodes commonly become the first site of metastasis. The diagnosis of metastatic lymph nodes is critical not only for staging tumors but also for planning following treatments.[158,159] In fact, MR imaging of lymph nodes enhanced by ultrasmall superparamagnetic iron oxide NPs was reported more than 10 years ago.[160] The mechanism largely relies on uptake of NPs by macrophages differently populated between benign and malignant nodes, but the efficacy remains to be improved. Gao and coworkers recently reported an alternative approach through active targeting of lymphatic metastasis.[28] To achieve this goal, they firstly established a reliable orthotopic gastric cancer animal model that enabled the occurrence of lymphatic metastasis contrasting to conventional subcutaneous tumor model. They then coated paramagnetic/upconversion $NaGdF_4$:Yb,Er crystals mentioned above with $NdGdF_4$ shell to effectively increase the upconversion luminescent efficiency, and on the other hand to facilitate MR imaging through Gd^{3+} ions on the particle surface. Also through the asymmetric PEG ligand, partly reduced anti-gastric cancer antibody MGb_2 was covalently attached to the particle surface to obtain an active targeting probe. The tumor-targeting ability of the resulting probe was verified by MRI and upconversion luminescence imaging after tail vein injection. Systematic studies further confirmed that primary tumor, lymphatic micrometastasis smaller than 1 mm, and omentum lymph node metastasis could optically be detected. More detailed results are summarized in **Figure 10**. In contrast, no benign lymph node exhibited detectable luminescence during the whole imaging time window, which can be attributed to the excellent anti-biofouling modification that prevents the nanoprobe from being taken up by benign lymph nodes.

^{99m}Tc-colloids are often used in the clinic for sensitively localizing the sentinel or first draining node through single-photon emission computed tomography (SPECT), followed by operation guided with Isosulfan blue for lymph node biopsy and resection. However, noninvasive imaging remains to be developed for localizing lymph nodes deep in the abdomen. Grimm and coworkers present a multimodal NP, i.e., ^{89}Zr-labeled commercial iron oxide particle-based contrast agent (Ferumoxytol), for sensitive detection of lymph nodes with positron emission tomography (PET)/MRI.[161] The imaging agent was prepared by covalently attaching desferrioxamine chelate to Ferumoxytol in the presence of ^{89}Zr ions. Through PET/MRI imaging studies on healthy and tumor-bearing mice, they demonstrated that the above NPs could be used for high resolution tomographic studies of lymphatic drainage in preclinical disease models. Nevertheless, purification is required before use due to the rapid degradation of the compound in vivo. Thus, robust radio-labeling of NPs remains to be solved irrespective of any in vivo applications. By incorporating metal radioisotope such as ^{111}In ions in the crystal lattice of Fe_3O_4, Gao's group reported biocompatible and non-leachable ^{111}In-labeled Fe_3O_4 NPs that can be potentially used for tumor as well as lymph node imaging through both MRI and SPECT.[162]

The malignant behaviors of cancers are strongly associated with tumor microenvironments that are characterized

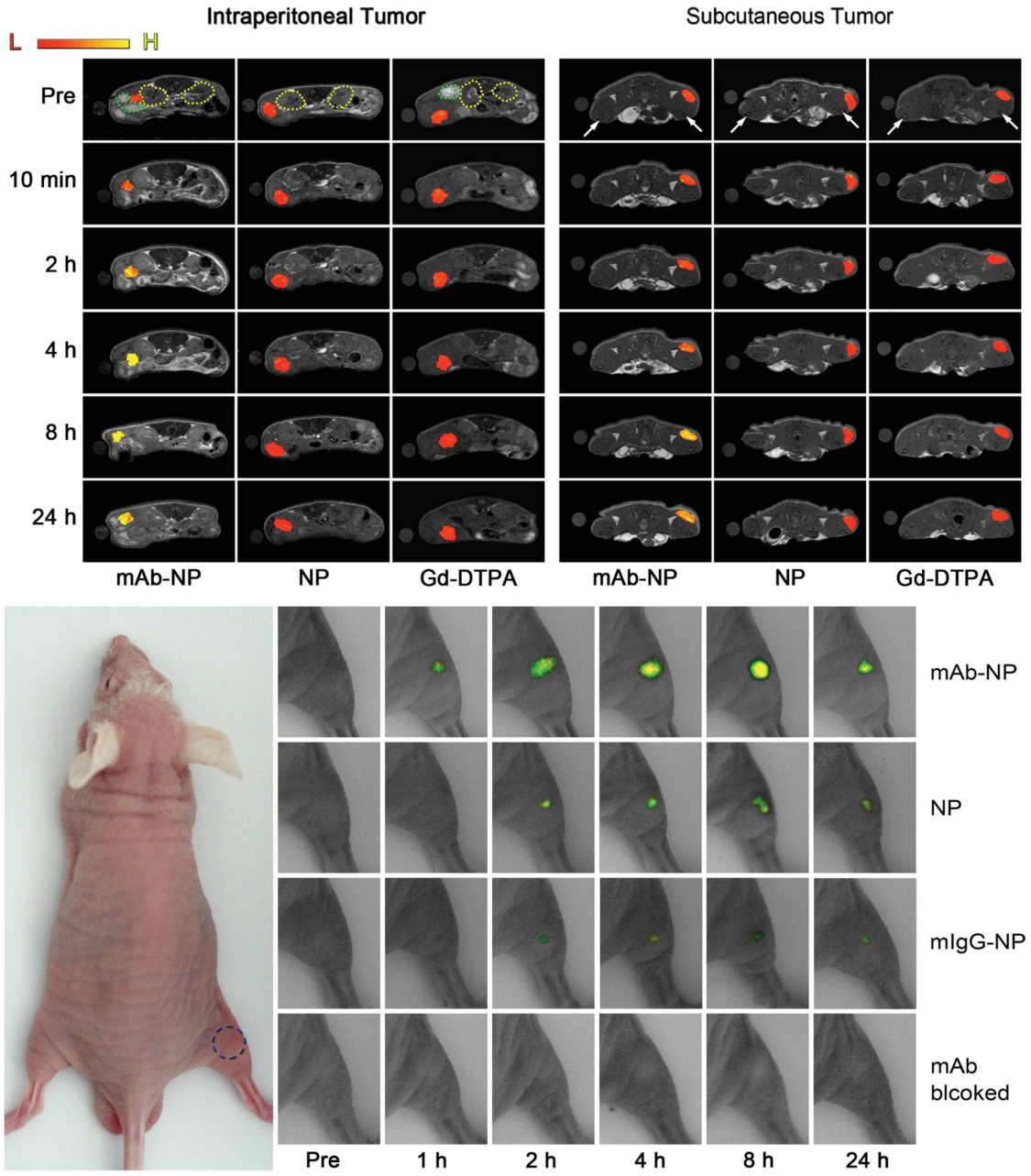

Figure 9. Upper panel: T_1-weighted MR images acquired before and at different time points after intravenously injecting mAb-NP probe, mother particle (NP), and Gd-DTPA into mice bearing intraperitoneally (left) and subcutaneously (right) transplanted tumors, respectively. The tumor sites are color-coded to better show the contrast enhancing effects, and organs such as kidney (encircled by yellow dotted line), stomach (encircled by green dotted line), and tibia (indicated by white arrows) are identified. Lower panel: An optical image of a nude mouse overlaid with a blue dashed circle indicating the 980 nm laser beam size for fully covering the xenografted tumors, and four sets of bright-field optical images of the tumor region overlaid with true-color upconversion fluorescence images recorded before and at different time points after intravenous injection of mAb-NP, NP, and mIgG-NP, respectively. The images captured in the cold mAb experiment are labeled "mAb blocked" and placed in the last row. Reproduced with permission.[18] Copyright 2013, American Chemical Society.

by abnormal expression of proteases, abnormal extracellular pH value, etc., which promote the proliferation, invasion, and metastasis of cancers. For example, matrix metalloproteases (MMPs), a family of zinc-dependent secreted endopeptidases, are involved in homeostatic regulation and processing of extracellular matrices. Their overexpression observed in tumors compromises extracellular matrix integrity and correlates with an advanced tumor stage, increased invasion and metastasis, and shortened survival. The acidic environment of malignant tumors correlates with a significant number of harmful consequences, such as increased invasion and mutation rates as well as radio resistance. Therefore, developing noninvasive methods for visualizing the tumor microenvironment is greatly meaningful for tumor studies on predicting metastasis potential, determining therapeutic efficacy, therapy development, and prognosis. Gao's group proposed

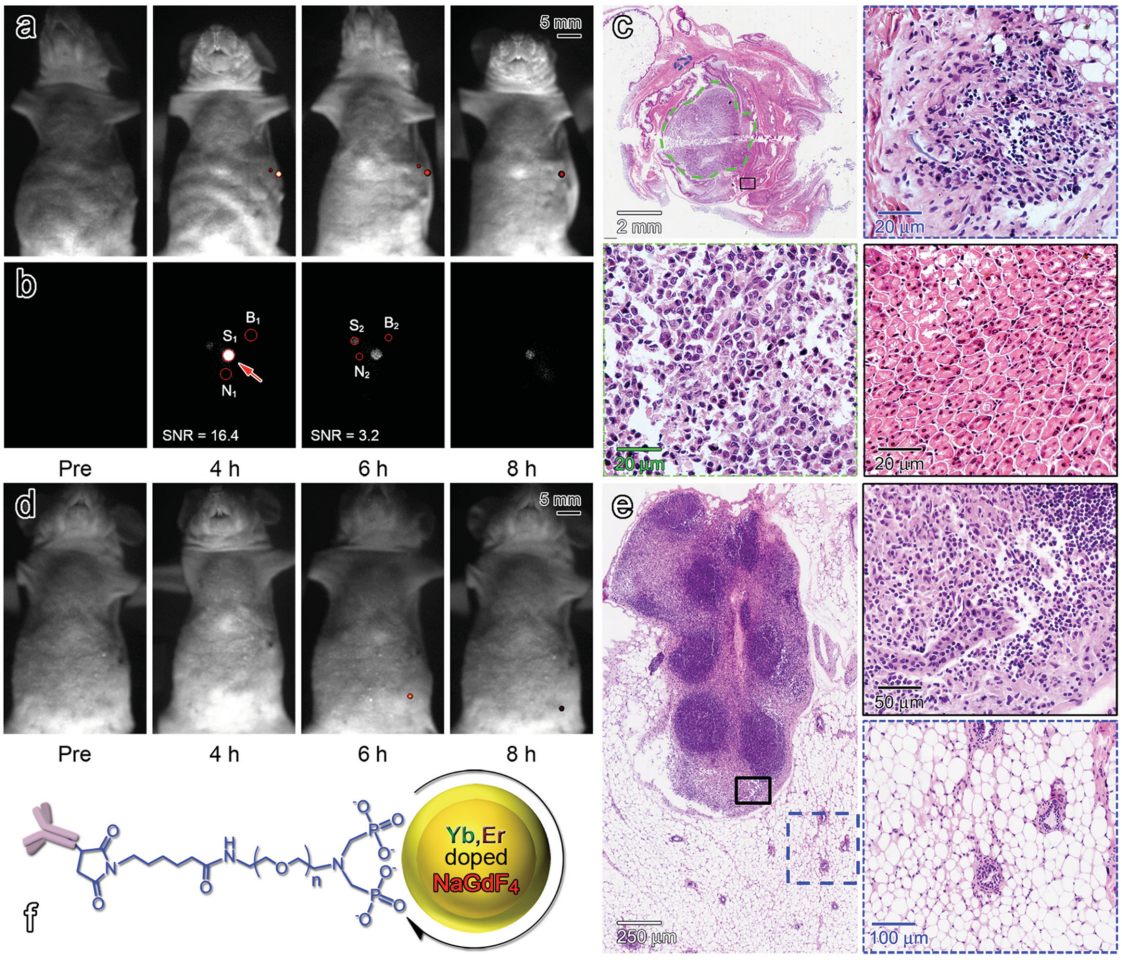

Figure 10. a) Optical images superimposed with color-coded upconversion luminescence images of the orthotopic tumor site obtained before and at different time points after intravenous injection of the NP-MGb_2 probe. b) Luminescence signals of the tumor site labeled with S for signal, N for noise, and B for background to determine signal-to-noise ratio (SNR). c) Histopathological images of the stomach showing two malignant lesions, i.e., the orthotopic tumor and its lymphatic micrometastasis highlighted by green and blue dashed lines, respectively, for comparing with normal stomach tissue in a solid black square, together with the enlarged images for these areas. d) In vivo optical images overlaided with upconversion luminescence images obtained before and at different time points after intravenous injection of the NP-MGb_2 probe into a purposely chosen mouse bearing smaller tumor. e) Histopathological image of the identified metastatic lymph node exhibiting upconversion luminescence. Part of the malignant node and the surrounding vasculature are enlarged to better show the metastatic characteristics. f) A cartoon picture showing the structure of the ultra-sensitive and gastric cancer specific probe constructed by covalently attaching mAb to the surface of PEGylated $NaGdF_4$:Yb, Er@$NaGdF_4$ core/shell particles. Reproduced with permission.[28] Copyright 2015, American Chemical Society.

a protease-activated fluorescence imaging probe based on Fe_3O_4 NPs and a covalently bonded pH-dependent ratiometric fluorescent dye, i.e., an *N*-carboxyhexyl derivative of 3-amino-1,2,4-triazole-fused 1,8-naphthalimide (ANNA).[16] In its 'off-state', the Fe_3O_4 particle quenched the fluorescence of ANNA, while the fluorophor ANNA was released upon the cleavage of the peptide linker by MMP-9, representing an 'on-state'. An on-state/off-state ratio factor of above 6 was achieved in vitro. Most importantly, the tumor-specific antibody on the dye side helped to firmly attach the fluorophor on cell membrane after the probe was activated, which makes it possible to detect the extracellular pH. The following in vivo animal imaging studies revealed that the above probe rapidly responded to the MMP-9 expressed in tumor, which promoted the visualization of the heterogeneity of tumors with respect to pH, as shown in **Figure 11**. Although enhanced MR imaging with the aid of the above probe carrier, i.e., Fe_3O_4 NPs, was not reported therein. In principle, it is surely helpful for providing more accurate anatomical information of the tumor. In fact, the chemical exchange saturation transfer has been used for MR imaging of tumor microenvironmental pH, but the above probe design is not limited solely to pH imaging.

Also for tumor imaging, effective crossing some biological barriers remains a hurdle for nanoprobes to overcome. For example, tumor stroma forms a barrier unfavorable for targeted drug delivery.[163–165] Previous studies reveal that over 86% of pancreatic cancer tissues express high levels of urokinase plasminogen activator receptor (uPAR) in tumor cells, tumor endothelial cells, and tumor stromal fibroblasts, and macrophages, while normal pancreas or pancreatic tissues with chronic pancreatitis do not express uPAR.[166,167] Most importantly, some drugs can break down tumor stromal fibroblasts and endothelial cells expressing uPAR. Towards

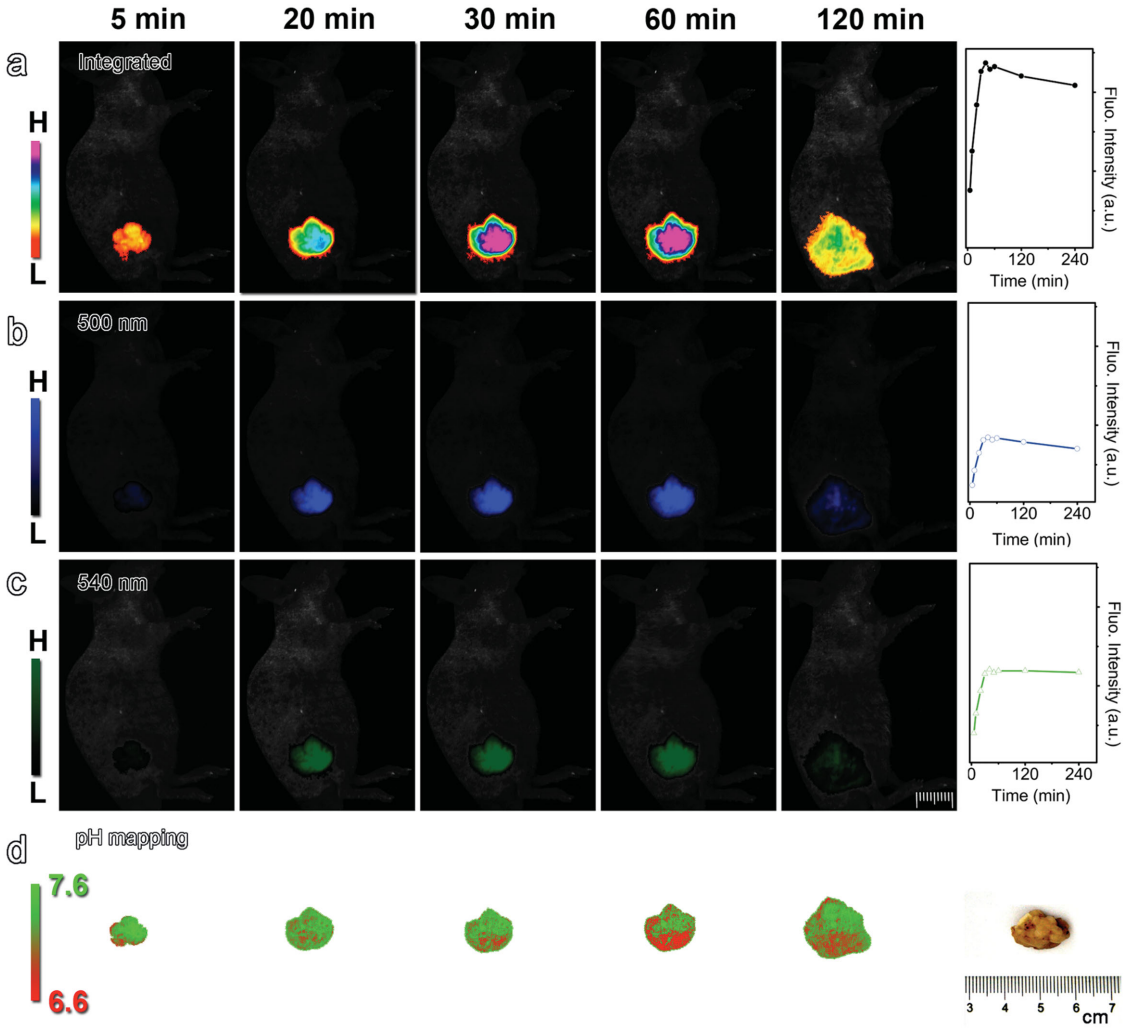

Figure 11. Color-coded fluorescence images of tumor-bearing mice based on emission of a) 500–600 nm, b) 500 nm, and c) 540 nm, with temporal variations of the integrated optical intensity lying aside. Pictures in row (d) show pH mapping of the tumor region with an optical image of the harvested tumor placed at right-hand side. Reproduced with permission.[16] Copyright 2015, American Chemical Society.

effective targeted drug delivery and imaging, Lily Yang and coworkers reported an uPAR-specific MRI probe by attaching a natural ligand of uPAR to the surface of magnetic iron oxide NPs apart from a tumor drug Gemcitabine linked through a lysosomal cleavable peptide.[168] Systematic studies in an orthotopic human pancreatic cancer xenograft model demonstrated that the above probe significantly inhibited tumor growth, suggesting that above uPAR-specific drug delivery system can overcome the stroma barriers. In addition, the presence of drug-resistant residual tumors could be detected noninvasively by T_2-weighted and T_1-weighted MR imaging with the aid of iron oxide NPs.

Brain tumors represented by glioblastoma multiforme (GBM) give rise to leading mortality and morbidity currently in children cancer patients.[169] In the brain, endothelial cells form a major physical and physiological barrier limiting the brain uptake of diagnostic and/or therapeutic agents.[170–172] Thus, targeted delivery across the BBB is one of the most challenging fields for diagnosis and therapy of brain tumors and various neurological disorder diseases as well. Iron oxide NPs have shown excellent contrast enhancement ability in MR imaging of brain with BBB impairment and/or inflammatory reactions,[173] yet strategies for delivering NPs across the BBB remain to be developed. Recently, Gao and coworkers reported a receptor-mediated strategy for overcoming intact BBB by covalently attaching lactoferrin (Lf) to a PEG-coated Fe_3O_4 NPs[124] based on the fact that the receptor of mammalian Lf, a cationic iron-binding glycoprotein, present on cerebral endothelial cells. The in vitro permeation experiments revealed that PEGylated Fe_3O_4 NPs had certain ability to pass through the BBB model owing to the amphiphilic nature of PEG coating, while the efficacy was increased by a factor of more than 2 for Fe_3O_4-Lf conjugate. The following in vitro blocking experiments suggested that Fe_3O_4-Lf conjugate crossed the BBB through receptor-mediated transcytosis, which was further supported by in vivo animal experiments. In addition to the transcytosis approach, temporarily opening of tight junction of BBB was also reported for across BBB delivery. Adenosine receptors are a class of G protein-coupled receptors including four subtypes of A_1, A_{2A}, A_{2B}, and A_3. The activation of the A_{2A} receptor expressed on brain capillary endothelial cells gives

rise to cytoskeleton modulation, cell shape contraction, and intercellular space enhencement, and leads to enhanced permeation across the BBB.[174] Based on this effect, a nanoprobe bearing regadenoson that has a moderate binding affinity to human A_{2A} adenosine receptors was reported for temporarily opening the BBB to achieve effective drug delivery.[175] Alternatively, it was recently demonstrated that high-intensity focused ultrasound can also temporarily open the BBB.[176,177] These approaches may open up new ways for delivering versatile nanoprobes across the BBB for brain imaging and theranotics.

5. Engineered versus Unintended Surface Coatings

The solution synthesis of colloidal NPs requires suitable surface capping agents to prevent the NPs from uncontrollable growth, and on the other hand to increase the colloidal stability of the NPs. Towards biomedical applications, biocompatible surface coatings are essentially required not only for colloidally stabilizing the NPs in physiological environments but also for offering reactive groups to further couple bioligands to enhance the accumulation of the particle probes in the region of interest.

Aiming at diagnostic imaging and/or therapeutic drug delivery, magnetic NPs are expected to be most commonly intravenously injected into the blood stream, at which point they inevitably interact biomolecules such as lipids, sugars and especially proteins that may subsequently adsorb onto the surface of NPs by certain degrees through by different types of interactions. The unintended formation of the biomolecule corona, typically termed the 'protein corona', may accelerate the clearance of them from the vascular compartment by the macrophages in the liver, the spleen, and the bone marrow, which are tissues belonging to the so-called reticuloendothelial system (RES). Such accumulation of the opsonized NPs into the RES organs is considered favorable when these organs are the intended target sites. However, for delivering the magnetic NPs to tissues other than the RES organs, minimizing the rapid systemic clearance of the NPs becomes essential.

Over the past years, great efforts have been paid, as summarized above and in previous review articles, to engineer the particle surface so as to increase the targeting ability of versatile functional inorganic NPs in vivo, yet unintended surface coating may persist in complex physiological environments.

The term of 'protein corona' was firstly introduced by Cedervall et al. in 2007.[178] The plasma protein corona has been shown to be highly complex.[179,180] Proteins involved in physiological as well as pathophysiological relevant processes in the blood system, such as complement activation and coagulation have been identified in the coronas of various NPs, including magnetic NPs.[180–188] Moreover, binding of opsonins such as IgG and complement factors are expected to promote rapid clearance of NPs. As dysopsonins, such as albumin, have been shown to prolong the nanoparticle circulation time in the blood, they may antagonize the biological reactions triggered by magnetic NPs bound opsonins.[180–182] Although detailed in vivo studies for the magnetic NPs are missing, one may speculate that an increase in the circulation time by bound dysopsonins may increase the contact with components of the coagulation system. A functionally diverse group of plasma proteins detectable in the corona of NPs are apolipoproteins that are involved in lipid and cholesterol transport and metabolism.[180,181] As apolipoproteins are able to bind to specific receptors, the apolipoproteins in the NPs' corona are expected to also affect their biodistribution.[180–182] Notably, the functionalization of NPs with certain apolipoproteins was reported to improve the NPs' ability to overcome biological barriers, such as the BBB.[189] Thus, magnetic NPs carrying an apolipoprotein-enriched protein corona signature may represent optimal candidates for brain imaging.

Since the protein corona is currently a still unpredictable factor, potentially triggering not only desired but also undesired biological reactions to NP probes, attempts to partially or completely prevent protein adsorption are currently intensively investigated.[184,190–194] Although PEGs are widely used to coat NPs for suppressing unwanted protein corona, recently studies revealed that PEGylation cannot completely prevent protein adsorption, albeit the extent of corona formation is clearly reduced.[181,184,190–194] An alternative method to the PEGylation is the functionalization of the NP surface with zwitterions.[195] As discussed, magnetic NPs with tunable hydrophobicity seem to attract very little plasma proteins, even at physiological serum concentration. Albeit these innovative strategies may lead to new generations of improved NPs, further developments for engineering 'corona-free' NPs need to be continued for increasing the targeting ability of versatile nanoprobes guided by specific ligands.

6. Conclusion

In comparison with small molecular MRI contrast agents, magnetic NPs, especially high quality iron oxide NPs and rare-earth NPs are considered as a promising generation of novel MRI contrast agents as they not only offer excellent relaxometric properties, active targeting ability through conjugation with versatile bioligands, and possibilities of multi-modality imaging and theranostics. Yet, the particle size tunability, impacts of surface modifications on the relaxometric properties of the underlying magnetic NPs, reliable surface chemistries for bioconjugation and prevention of the formation of protein coronas as well, reproducibility of NPs' production, and proper choice of the materials remains critical subjects not only meaningful for fundamental studies but also for translational medicine. The Precision Medicine Initiative launched by the US sets cancer therapeutics as a short term goal, which will provide excellent opportunities for nanomedicine. Fruitful achievements are however only expected upon collaborations pulled by clinicians, and pushed by physicists, chemists, material scientists, meanwhile with the continuous support of biologists involved to find relevant biomarkers and pathological mechanisms for accurately pinpointing cancerous areas and developing effective tumor theranostic strategies.

Acknowledgements

E.Y.Z. and R.H.S. contributed equally to this work. The authors thank the National Basic Research Program of China (2011CB935800), the National Natural Science Foundation of China (81090271, 21321063), ICCAS (CMS-PY-201309), BMBF-NanoBEL (DFG-SPP1313) for financial support. R.H.S. acknowledges the financial support of CAS President's International Fellowship Initiative (PIFI) (2015VMA001).

[1] P. D. Howes, R. Chandrawati, M. M. Stevens, *Science* **2014**, *346*, 53.
[2] C. Y. Liu, Y. Hou, M. Y. Gao, *Adv. Mater.* **2014**, *26*, 6922.
[3] C. Li, *Nat. Mater.* **2014**, *13*, 110.
[4] N. Lee, T. Hyeon, *Chem. Soc. Rev.* **2012**, *41*, 2575.
[5] J. Estelrich, E. Escribano, J. Queralt, M. A. Busquets, *Int. J. Mol. Sci.* **2015**, *16*, 8070.
[6] D. S. Ling, T. Hyeon, *Small* **2013**, *9*, 1450.
[7] G. Palui, F. Aldeek, W. T. Wang, H. Mattoussi, *Chem. Soc. Rev.* **2015**, *44*, 193.
[8] Z. C. Sun, X. X. Song, X. J. Li, T. Su, S. Qi, R. R. Qiao, F. Wang, Y. Huan, W. D. Yang, J. Wang, Y. Z. Nie, K. C. Wu, M. Y. Gao, F. Cao, *Nanoscale* **2014**, *6*, 14343.
[9] S. Dutz, R. Hergt, *Nanotechnology* **2014**, *25*, 28.
[10] C. L. Degen, M. Poggio, H. J. Mamin, C. T. Rettner, D. Rugar, *Proc. Nat. Acad. Sci. USA* **2009**, *106*, 1313.
[11] R. Weissleder, M. Nahrendorf, M. J. Pittet, *Nat. Mater.* **2014**, *13*, 125.
[12] R. Qiao, C. Yang, M. Gao, *J. Mater. Chem.* **2009**, *19*, 9286.
[13] H. S. Thomsen, S. K. Morcos, P. Dawson, *Clin. Radiol.* **2006**, *61*, 905.
[14] J. R. Alger, J. H. Harreld, S. Chen, J. Mintorovitch, D. S. K. Lu, *J. Magn. Reson. Imaging* **2001**, *14*, 586.
[15] A. Albanese, P. S. Tang, W. C. W. Chan, *Annu. Rev. Biomed. Eng.* **2012**, *14*, 1.
[16] Y. Hou, J. Zhou, Z. Gao, X. Sun, C. Liu, D. Shangguan, W. Yang, M. Gao, *ACS Nano* **2015**, *9*, 3199.
[17] J. F. Zeng, L. H. Jing, Y. Hou, M. X. Jiao, R. R. Qiao, Q. J. Jia, C. Y. Liu, F. Fang, H. Lei, M. Y. Gao, *Adv. Mater.* **2014**, *26*, 2694.
[18] C. Y. Liu, Z. Y. Gao, J. F. Zeng, Y. Hou, F. Fang, Y. L. Li, R. R. Qiao, L. Shen, H. Lei, W. S. Yang, M. Y. Gao, *ACS Nano* **2013**, *7*, 7227.
[19] E. Y. Zhao, Z. X. Zhao, J. C. Wang, C. H. Yang, C. J. Chen, L. Y. Gao, Q. Feng, W. J. Hou, M. Y. Gao, Q. Zhang, *Nanoscale* **2012**, *4*, 5102.
[20] Y. L. Li, X. Duan, L. H. Jing, C. H. Yang, R. R. Qiao, M. Y. Gao, *Biomaterials* **2011**, *32*, 1923.
[21] M. Jiao, J. Zeng, L. Jing, C. Liu, M. Gao, *Chem. Mater.* **2015**, *27*, 1299.
[22] B. H. Kim, N. Lee, H. Kim, K. An, Y. I. Park, Y. Choi, K. Shin, Y. Lee, S. G. Kwon, H. B. Na, J. G. Park, T. Y. Ahn, Y. W. Kim, W. K. Moon, S. H. Choi, T. Hyeon, *J. Am. Chem. Soc.* **2011**, *133*, 12624.
[23] P. Caravan, J. J. Ellison, T. J. Mcmurry, R. B. Lauffer, *Chem. Rev.* **1999**, *99*, 2293.
[24] J. Chanyaputhipong, S.-C. A. Low, P. K. H. Chow, *Int. J. Hepatol.* **2011**, *2011*, 489342.
[25] M. Lewis, S. Yanny, P. N. Malcolm, *J. Med. Imag. Radiat. Oncol.* **2012**, *56*, 187.
[26] C. Dong, A. Korinek, B. Blasiak, B. Tomanek, F. C. J. M. Van Veggel, *Chem. Mater.* **2012**, *24*, 1297.
[27] L. Sandiford, A. Phinikaridou, A. Protti, L. K. Meszaros, X. J. Cui, Y. Yan, G. Frodsham, P. A. Williamson, N. Gaddum, R. M. Botnar, P. J. Blower, M. A. Green, R. T. M. De Rosales, *ACS Nano* **2013**, *7*, 500.
[28] R. R. Qiao, C. H. Liu, M. H. Liu, H. Hu, C. Y. Liu, Y. Hou, K. C. Wu, Y. N. Lin, J. M. Liang, M. Y. Gao, *ACS Nano* **2015**, *9*, 2120.
[29] Z. Liu, K. Dong, J. H. Liu, X. L. Han, J. S. Ren, X. G. Qu, *Small* **2014**, *10*, 2429.
[30] C. Feldmann, H. O. Jungk, *Angew. Chem., Int. Ed.* **2001**, *40*, 359.
[31] C. Feldmann, *Adv. Funct. Mater.* **2003**, *13*, 101.
[32] J. L. Bridot, A. C. Faure, S. Laurent, C. Riviere, C. Billotey, B. Hiba, M. Janier, V. Josserand, J. L. Coll, L. Vander Elst, R. Muller, S. Roux, P. Perriat, O. Tillement, *J. Am. Chem. Soc.* **2007**, *129*, 5076.
[33] R. Bazzi, M. A. Flores, C. Louis, K. Lebbou, W. Zhang, C. Dujardin, S. Roux, B. Mercier, G. Ledoux, E. Bernstein, P. Perriat, O. Tillement, *J. Colloid Interface Sci.* **2004**, *273*, 191.
[34] H. Guo, N. Dong, M. Yin, W. P. Zhang, L. R. Lou, S. D. Xia, *J. Phys. Chem. B* **2004**, *108*, 19205.
[35] H. X. Mai, Y. W. Zhang, R. Si, Z. G. Yan, L. D. Sun, L. P. You, C. H. Yan, *J. Am. Chem. Soc.* **2006**, *128*, 6426.
[36] M. J. Cho, R. Sethi, J. S. A. Narayanan, S. S. Lee, D. N. Benoit, N. Taheri, P. Decuzzi, V. L. Colvin, *Nanoscale* **2014**, *6*, 13637.
[37] T. Paik, T. R. Gordon, A. M. Prantner, H. Yun, C. B. Murray, *ACS Nano* **2013**, *7*, 2850.
[38] Y. I. Park, J. H. Kim, K. T. Lee, K. S. Jeon, H. Bin Na, J. H. Yu, H. M. Kim, N. Lee, S. H. Choi, S. I. Baik, H. Kim, S. P. Park, B. J. Park, Y. W. Kim, S. H. Lee, S. Y. Yoon, I. C. Song, W. K. Moon, Y. D. Suh, T. Hyeon, *Adv. Mater.* **2009**, *21*, 4467.
[39] X. F. Qiao, J. C. Zhou, J. W. Xiao, Y. F. Wang, L. D. Sun, C. H. Yan, *Nanoscale* **2012**, *4*, 4611.
[40] C. Li, D. Yang, P. A. Ma, Y. Chen, Y. Wu, Z. Hou, Y. Dai, J. Zhao, C. Sui, J. Lin, *Small* **2013**, *9*, 4150.
[41] Z. Q. Li, Y. Zhang, *Nanotechnology* **2008**, *19*, 345606.
[42] Z. Q. Li, Y. Zhang, S. Jiang, *Adv. Mater.* **2008**, *20*, 4765.
[43] N. J. J. Johnson, W. Oakden, G. J. Stanisz, R. S. Prosser, F. C. J. M. Van Veggel, *Chem. Mater.* **2011**, *23*, 4877.
[44] Y. Hou, R. R. Qiao, F. Fang, X. X. Wang, C. Y. Dong, K. Liu, C. Y. Liu, Z. F. Liu, H. Lei, F. Wang, M. Y. Gao, *ACS Nano* **2013**, *7*, 330.
[45] F. Chen, W. B. Bu, S. J. Zhang, X. H. Liu, J. N. Liu, H. Y. Xing, Q. F. Xiao, L. P. Zhou, W. J. Peng, L. Z. Wang, J. L. Shi, *Adv. Funct. Mater.* **2011**, *21*, 4285.
[46] I. Mcgill, in *Ullmann's Encyclopedia of Industrial Chemistry*, Wiley-VCH, Weinheim, Germany, **2000**.
[47] A. Palasz, P. Czekaj, *Acta Biochim. Pol.* **2000**, *47*, 1107.
[48] L. C. Adding, G. L. Bannenberg, L. E. Gustafsson, *Cardiovasc. Drug Rev.* **2001**, *19*, 41.
[49] R. B. Lauffer, *Chem. Rev.* **1987**, *87*, 901.
[50] K. Riley, FDA Requests Boxed Warning for Contrast Agents Used to Improve MRI Images, **2007**. http://www.fda.gov/NewsEvents/Newsroom/PressAnnouncements/2007/ucm108919.htm (accessed: May 23).
[51] Y. F. Wang, L. D. Sun, J. W. Xiao, W. Feng, J. C. Zhou, J. Shen, C. H. Yan, *Chem. – Eur. J.* **2012**, *18*, 5558.
[52] H. J. Weinmann, R. C. Brasch, W. R. Press, G. E. Wesbey, *Am. J. Roentgenol.* **1984**, *142*, 619.
[53] L. Q. Xiong, T. S. Yang, Y. Yang, C. J. Xu, F. Y. Li, *Biomaterials* **2010**, *31*, 7078.
[54] Y. Park, H. M. Kim, J. H. Kim, K. C. Moon, B. Yoo, K. T. Lee, N. Lee, Y. Choi, W. Park, D. Ling, K. Na, W. K. Moon, S. H. Choi, H. S. Park, S. Y. Yoon, Y. D. Suh, S. H. Lee, T. Hyeon, *Adv. Mater.* **2012**, *24*, 5755.
[55] L. Q. Xiong, Z. G. Chen, Q. W. Tian, T. Y. Cao, C. J. Xu, F. Y. Li, *Anal. Chem.* **2009**, *81*, 8687.
[56] L. Q. Xiong, Z. G. Chen, M. X. Yu, F. Y. Li, C. Liu, C. H. Huang, *Biomaterials* **2009**, *30*, 5592.
[57] J. Lee, T. S. Lee, J. Ryu, S. Hong, M. Kang, K. Im, J. H. Kang, S. M. Lim, S. Park, R. Song, *J. Nucl. Med.* **2013**, *54*, 96.

[58] R. A. Jalil, Y. Zhang, *Biomaterials* **2008**, *29*, 4122.
[59] Y. Yang, Y. Sun, Y. Liu, J. J. Peng, Y. Q. Wu, Y. J. Zhang, W. Feng, F. Y. Li, *Biomaterials* **2013**, *34*, 508.
[60] M. Thuen, M. Berry, T. B. Pedersen, P. E. Goa, M. Summerfield, O. Haraldseth, A. Sandvig, C. Brekken, *J. Magn. Reson. Imaging* **2008**, *28*, 855.
[61] Y.-T. Kuo, A. H. Herlihy, P.-W. So, J. D. Bell, *NMR Biomed.* **2006**, *19*, 1028.
[62] A. Gozzi, A. Schwarz, V. Crestan, A. Bifone, *Proc. Intl. Soc. Mag. Reson. Med.* **2008**, *16*, 2314.
[63] D. C. Borg, G. C. Cotzias, *J. Clin. Invest.* **1958**, *37*, 1269.
[64] Cl. Witzlebe, *Am. J. Pathol.* **1969**, *57*, 617.
[65] I. Mena, O. Marin, S. Fuenzali, G. C. Cotzias, *Neurology* **1967**, *17*, 128.
[66] J. Sorvari, M. Sillanpaa, *Chemosphere* **1996**, *33*, 1119.
[67] G. Elizondo, C. J. Fretz, D. D. Stark, S. M. Rocklage, S. C. Quay, D. Worah, Y. M. Tsang, M. C. M. Chen, J. T. Ferrucci, *Radiology* **1991**, *178*, 73.
[68] D. Pan, A. H. Schmieder, S. A. Wickline, G. M. Lanza, *Tetrahedron* **2011**, *67*, 843.
[69] K. Ding, L. H. Jing, C. Y. Liu, Y. Hou, M. Y. Gao, *Biomaterials* **2014**, *35*, 1608.
[70] L. H. Jing, K. Ding, S. Kalytchuk, Y. Wang, R. R. Qiao, S. V. Kershaw, A. L. Rogach, M. Y. Gao, *J. Phys. Chem. C* **2013**, *117*, 18752.
[71] L. H. Jing, K. Ding, S. V. Kershaw, I. M. Kempson, A. L. Rogach, M. Y. Gao, *Adv. Mater.* **2014**, *26*, 6367.
[72] Y. F. Chen, E. Johnson, X. G. Peng, *J. Am. Chem. Soc.* **2007**, *129*, 10937.
[73] Y. W. Tan, L. R. Meng, Q. Peng, Y. D. Li, *Chem. Commun.* **2011**, *47*, 1172.
[74] H. W. Zhang, L. H. Jing, J. F. Zeng, Y. Hou, Z. Li, M. Y. Gao, *Nanoscale* **2014**, *6*, 5918.
[75] W. S. Seo, H. H. Jo, K. Lee, B. Kim, S. J. Oh, J. T. Park, *Angew. Chem., Int. Ed.* **2004**, *43*, 1115.
[76] F. Jiao, A. Harrison, P. G. Bruce, *Angew. Chem., Int. Ed.* **2007**, *46*, 3946.
[77] X. Sun, Y. W. Zhang, R. Si, C. H. Yan, *Small* **2005**, *1*, 1081.
[78] M. Yin, S. O'Brien, *J. Am. Chem. Soc.* **2003**, *125*, 10180.
[79] J. Park, K. J. An, Y. S. Hwang, J. G. Park, H. J. Noh, J. Y. Kim, J. H. Park, N. M. Hwang, T. Hyeon, *Nat. Mater.* **2004**, *3*, 891.
[80] D. Zitoun, N. Pinna, N. Frolet, C. Belin, *J. Am. Chem. Soc.* **2005**, *127*, 15034.
[81] K. An, M. Park, J. H. Yu, H. B. Na, N. Lee, J. Park, S. H. Choi, I. C. Song, W. K. Moon, T. Hyeon, *Eur. J. Inorg. Chem.* **2012**, 2148.
[82] T. D. Schladt, T. Graf, W. Tremel, *Chem. Mater.* **2009**, *21*, 3183.
[83] P. Li, C. Y. Nan, Z. Wei, J. Lu, Q. Peng, Y. D. Li, *Chem. Mater.* **2010**, *22*, 4232.
[84] K. An, S. G. Kwon, M. Park, H. B. Na, S. I. Baik, J. H. Yu, D. Kim, J. S. Son, Y. W. Kim, I. C. Song, W. K. Moon, H. M. Park, T. Hyeon, *Nano Letters* **2008**, *8*, 4252.
[85] T. Kim, E.-J. Cho, Y. Chae, M. Kim, A. Oh, J. Jin, E.-S. Lee, H. Baik, S. Haam, J.-S. Suh, Y.-M. Huh, K. Lee, *Angew. Chem., Int. Ed.* **2011**, *50*, 10589.
[86] H. Si, H. Wang, H. Shen, C. Zhou, S. Li, S. Lou, W. Xu, Z. Du, L. S. Li, *CrystEngComm* **2009**, *11*, 1128.
[87] X. H. Zhong, R. G. Xie, L. T. Sun, I. Lieberwirth, W. Knoll, *J. Phys. Chem. B* **2006**, *110*, 2.
[88] M. Park, N. Lee, S. H. Choi, K. An, S. H. Yu, J. H. Kim, S. H. Kwon, D. Kim, H. Kim, S. I. Baek, T. Y. Ahn, O. K. Park, J. S. Son, Y. E. Sung, Y. W. Kim, Z. W. Wang, N. Pinna, T. Hyeon, *Chem. Mater.* **2011**, *23*, 3318.
[89] T. Ould-Ely, D. Prieto-Centurion, A. Kumar, W. Guo, W. V. Knowles, S. Asokan, M. S. Wong, I. Rusakova, A. Luttge, K. H. Whitmire, *Chem. Mater.* **2006**, *18*, 1821.
[90] A. Naravanaswamy, H. F. Xu, N. Pradhan, X. G. Peng, *Angew. Chem., Int. Ed.* **2006**, *45*, 5361.
[91] T. Yu, J. Moon, J. Park, Y. I. Park, H. Bin Na, B. H. Kim, I. C. Song, W. K. Moon, T. Hyeon, *Chem. Mater.* **2009**, *21*, 2272.
[92] H. B. Na, J. H. Lee, K. J. An, Y. I. Park, M. Park, I. S. Lee, D. H. Nam, S. T. Kim, S. H. Kim, S. W. Kim, K. H. Lim, K. S. Kim, S. O. Kim, T. Hyeon, *Angew. Chem., Int. Ed.* **2007**, *46*, 5397.
[93] J. Shin, R. M. Anisur, M. K. Ko, G. H. Im, J. H. Lee, I. S. Lee, *Angew. Chem., Int. Ed.* **2009**, *48*, 321.
[94] Z. J. Liu, X. X. Song, Q. Tang, *Nanoscale* **2013**, *5*, 5073.
[95] Z. L. Zhao, H. H. Fan, G. F. Zhou, H. R. Bai, H. Liang, R. W. Wang, X. B. Zhang, W. H. Tan, *J. Am. Chem. Soc.* **2014**, *136*, 11220.
[96] L. Wang, Q. Wu, S. Tang, J. Zeng, R. Qiao, P. Zhao, Y. Zhang, F. Hu, M. Gao, *RSC Adv.* **2013**, *3*, 23454.
[97] J. W. M. Bulte, D. L. Kraitchman, *NMR Biomed.* **2004**, *17*, 484.
[98] R. R. Qiao, J. F. Zeng, Q. J. Jia, J. Du, L. Shen, M. Y. Gao, *Acta Phys.-Chim. Sin.* **2012**, *28*, 993.
[99] J. Rockenberger, E. C. Scher, A. P. Alivisatos, *J. Am. Chem. Soc.* **1999**, *121*, 11595.
[100] D. Kim, N. Lee, M. Park, B. H. Kim, K. An, T. Hyeon, *J. Am. Chem. Soc.* **2009**, *131*, 454.
[101] S. H. Sun, H. Zeng, D. B. Robinson, S. Raoux, P. M. Rice, S. X. Wang, G. X. Li, *J. Am. Chem. Soc.* **2004**, *126*, 273.
[102] N. R. Jana, Y. F. Chen, X. G. Peng, *Chem. Mater.* **2004**, *16*, 3931.
[103] Z. Li, H. Chen, H. B. Bao, M. Y. Gao, *Chem. Mater.* **2004**, *16*, 1391.
[104] Z. Li, Q. Sun, M. Y. Gao, *Angew. Chem., Int. Ed.* **2005**, *44*, 123.
[105] X. Y. Lu, M. Niu, R. R. Qiao, M. Y. Gao, *J. Phys. Chem. B* **2008**, *112*, 14390.
[106] X. Lu, M. Niu, C. Yang, L. Yi, R. Qiao, M. Du, M. Gao, *Chin. Sci. Bull.* **2010**, *55*, 3472.
[107] Z. Li, L. Wei, M. Y. Gao, H. Lei, *Adv. Mater.* **2005**, *17*, 1001.
[108] F. Q. Hu, Z. Li, C. F. Tu, M. Y. Gao, *J. Colloid Interface Sci.* **2007**, *311*, 469.
[109] F. Q. Hu, L. Wei, Z. Zhou, Y. L. Ran, Z. Li, M. Y. Gao, *Adv. Mater.* **2006**, *18*, 2553.
[110] S. J. Liu, B. Jia, R. R. Qiao, Z. Yang, Z. L. Yu, Z. F. Liu, K. Liu, J. Y. Shi, O. Y. Han, F. Wang, M. Y. Gao, *Mol. Pharmaceutics* **2009**, *6*, 1074.
[111] S. J. Liu, Y. C. Han, R. R. Qiao, J. F. Zeng, Q. J. Jia, Y. L. Wang, M. Y. Gao, *J. Phys. Chem. C* **2010**, *114*, 21270.
[112] Q. J. Jia, J. F. Zeng, R. R. Qjao, L. H. Jing, L. Peng, F. L. Gu, M. Y. Gao, *J. Am. Chem. Soc.* **2011**, *133*, 19512.
[113] W. Han, L. X. Yi, N. Zhao, A. W. Tang, M. Y. Gao, Z. Y. Tang, *J. Am. Chem. Soc.* **2008**, *130*, 13152.
[114] J. Lynch, J. Q. Zhuang, T. Wang, D. Lamontagne, H. M. Wu, C. Cao, *J. Am. Chem. Soc.* **2011**, *133*, 12664.
[115] N. Lee, Y. Choi, Y. Lee, M. Park, W. K. Moon, S. H. Choi, T. Hyeon, *Nano Lett.* **2012**, *12*, 3127.
[116] E. D. Smolensky, H. Y. E. Park, Y. Zhou, G. A. Rolla, M. Marjanska, M. Botta, V. C. Pierre, *J. Mater. Chem. B* **2013**, *1*, 2818.
[117] Z. Zhao, Z. Zhou, J. Bao, Z. Wang, J. Hu, X. Chi, K. Ni, R. Wang, X. Chen, Z. Chen, J. Gao, *Nat. Commun.* **2013**, *4*, 2266.
[118] R. H. Kodama, *J. Magn. Magn. Mater.* **1999**, *200*, 359.
[119] U. I. Tromsdorf, O. T. Bruns, S. C. Salmen, U. Beisiegel, H. Weller, *Nano Lett.* **2009**, *9*, 4434.
[120] F. Q. Hu, Q. J. Jia, Y. L. Li, M. Y. Gao, *Nanotechnology* **2011**, *22*, 245604.
[121] Z. Li, P. W. Yi, Q. Sun, H. Lei, H. L. Zhao, Z. H. Zhu, S. C. Smith, M. B. Lan, G. Q. Lu, *Adv. Funct. Mater.* **2012**, *22*, 2387.
[122] E. Taboada, E. Rodriguez, A. Roig, J. Oro, A. Roch, R. N. Muller, *Langmuir* **2007**, *23*, 4583.
[123] Q. L. Vuong, J. F. Berret, J. Fresnais, Y. Gossuin, O. Sandre, *Adv. Healthcare Mater.* **2012**, *1*, 502.
[124] R. R. Qiao, Q. J. Jia, S. Huwel, R. Xia, T. Liu, F. B. Gao, H. J. Galla, M. Y. Gao, *ACS Nano* **2012**, *6*, 3304.
[125] C. Yang, H. Zhao, Y. Hou, D. Ma, *J. Am. Chem. Soc.* **2012**, *134*, 15814.
[126] J. Yu, C. Yang, J. D. S. Li, Y. C. Ding, L. Zhang, M. Z. Yousaf, J. Lin, R. Pang, L. B. Wei, L. L. Xu, F. G. Sheng, C. H. Li, G. J. Li, L. Y. Zhao, Y. L. Hou, *Adv. Mater.* **2014**, *26*, 4114.

[127] G. Huang, J. Hu, H. Zhang, Z. Zhou, X. Chi, J. Gao, *Nanoscale* **2014**, *6*, 726.
[128] W. W. Yu, E. Chang, J. C. Falkner, J. Zhang, A. M. Al-Somali, C. M. Sayes, J. Johns, R. Drezek, V. L. Colvin, *J. Am. Chem. Soc.* **2007**, *129*, 2871.
[129] H. Wu, H. Zhu, J. Zhuang, S. Yang, C. Liu, Y. C. Cao, *Angew. Chem., Int. Ed.* **2008**, *47*, 3730.
[130] C. A. J. Lin, R. A. Sperling, J. K. Li, T. Y. Yang, P. Y. Li, M. Zanella, W. H. Chang, W. G. J. Parak, *Small* **2008**, *4*, 334.
[131] N. Lee, H. R. Cho, M. H. Oh, S. H. Lee, K. Kim, B. H. Kim, K. Shin, T.-Y. Ahn, J. W. Choi, Y.-W. Kim, S. H. Choi, T. Hyeon, *J. Am. Chem. Soc.* **2012**, *134*, 10309.
[132] J. C. Li, Y. Hu, J. Yang, P. Wei, W. J. Sun, M. W. Shen, G. X. Zhang, X. Y. Shi, *Biomaterials* **2015**, *38*, 10.
[133] V. Amendola, S. Scaramuzza, L. Litti, M. Meneghetti, G. Zuccolotto, A. Rosato, E. Nicolato, P. Marzola, G. Fracasso, C. Anselmi, M. Pinto, M. Colombatti, *Small* **2014**, *10*, 2476.
[134] J. Kim, H. S. Kim, N. Lee, T. Kim, H. Kim, T. Yu, I. C. Song, W. K. Moon, T. Hyeon, *Angew. Chem., Int. Ed.* **2008**, *47*, 8438.
[135] J. Zhou, Y. Sun, X. Du, L. Xiong, H. Hu, F. Li, *Biomaterials* **2010**, *31*, 3287.
[136] H. P. Zhou, C. H. Xu, W. Sun, C. H. Yan, *Adv. Funct. Mater.* **2009**, *19*, 3892.
[137] J. Zhou, Y. Sun, X. X. Du, L. Q. Xiong, H. Hu, F. Y. Li, *Biomaterials* **2010**, *31*, 3287.
[138] Y. Liu, T. Chen, C. C. Wu, L. P. Qiu, R. Hu, J. Li, S. Cansiz, L. Q. Zhang, C. Cui, G. Z. Zhu, M. X. You, T. Zhang, W. H. Tan, *J. Am. Chem. Soc.* **2014**, *136*, 12552.
[139] H. Wei, N. Insin, J. Lee, H. S. Han, J. M. Cordero, W. H. Liu, M. G. Bawendi, *Nano Letters* **2012**, *12*, 22.
[140] X. Liu, H. Huang, Q. Jin, J. Ji, *Langmuir* **2011**, *27*, 5242.
[141] A. G. Dong, X. C. Ye, J. Chen, Y. J. Kang, T. Gordon, J. M. Kikkawa, C. B. Murray, *J. Am. Chem. Soc.* **2011**, *133*, 998.
[142] S. Wen, D. F. Liu, Z. Liu, S. Harris, Y. Y. Yao, Q. Ding, F. Nie, T. Lu, H. J. Chen, Y. L. An, F. C. Zang, G. J. Teng, *J. Lipid Res.* **2012**, *53*, 829.
[143] S. Wen, D. F. Liu, Y. Cui, S. S. Harris, Y. C. Chen, K. C. Li, S. H. Ju, G. J. Teng, *J. Nanomed. Nanotechnol.* **2014**, *10*, 639.
[144] D. P. Cormode, E. Roessl, A. Thran, T. Skajaa, R. E. Gordon, J.-P. Schlomka, V. Fuster, E. A. Fisher, W. J. M. Mulder, R. Proksa, Z. A. Fayad, *Radiology* **2010**, *256*, 774.
[145] M. E. Kooi, V. C. Cappendijk, K. Cleutjens, A. G. H. Kessels, P. Kitslaar, M. Borgers, P. M. Frederik, M. Daemen, J. M. A. Van Engelshoven, *Circulation* **2003**, *107*, 2453.
[146] W. Koenig, N. Khuseyinova, *Arterioscler., Thromb., Vasc. Biol.* **2007**, *27*, 15.
[147] T. Y. Tang, S. P. S. Howarth, S. R. Miller, M. J. Graves, A. J. Patterson, J.-M. U-King-Im, Z. Y. Li, S. R. Walsh, A. P. Brown, P. J. Kirkpatrick, E. A. Warburton, P. D. Hayes, K. Varty, J. R. Boyle, M. E. Gaunt, A. Zalewski, J. H. Gillard, *J. Am. Coll. Cardiol.* **2009**, *53*, 2039.
[148] D. Fayol, N. Luciani, L. Lartigue, F. Gazeau, C. Wilhelm, *Adv. Healthcare Mater.* **2013**, *2*, 313.
[149] J. H. Zhu, L. F. Zhou, F. G. Xingwu, *N. Engl. J. Med.* **2006**, *355*, 2376.
[150] X. Zhang, S. N. De Chickera, C. Willert, V. Economopoulos, J. Noad, R. Rohani, A. Y. Wang, M. K. Levings, E. Scheid, R. Foley, P. J. Foster, G. A. Dekaban, *Cytotherapy* **2011**, *13*, 1234.
[151] J. Xie, J. H. Wang, G. Niu, J. Huang, K. Chen, X. G. Li, X. Y. Chen, *Chem. Commun.* **2010**, *46*, 433.
[152] T. Kim, E. Momin, J. Choi, K. Yuan, H. Zaidi, J. Kim, M. Park, N. Lee, M. T. Mcmahon, A. Quinones-Hinojosa, J. W. M. Bulte, T. Hyeon, A. A. Gilad, *J. Am. Chem. Soc.* **2011**, *133*, 2955.
[153] D. Peer, J. M. Karp, S. Hong, O. C. Farokhzad, R. Margalit, R. Langer, *Nat. Nanotechnol.* **2007**, *2*, 751.
[154] S. H. Sun, *J. Inorg. Organomet. Polym. Mater.* **2014**, *24*, 33.
[155] P. Sharma, N. E. Bengtsson, G. A. Walter, H. B. Sohn, G. Y. Zhou, N. Iwakuma, H. D. Zeng, S. R. Grobmyer, E. W. Scott, B. M. Moudgil, *Small* **2012**, *8*, 2856.
[156] S. Aryal, J. Key, C. Stigliano, M. D. Landis, D. Y. Lee, P. Decuzzi, *Small* **2014**, *10*, 2688.
[157] C. Kaittanis, T. M. Shaffer, A. Ogirala, S. Santra, J. M. Perez, G. Chiosis, Y. Li, L. Josephson, J. Grimm, *Nat. Commun.* **2014**, *5*, 3384.
[158] M. Harisinghani, J. Barentsz, R. Weissleder, *N. Engl. J. Med.* **2003**, *349*, 1186.
[159] V. Q. Hieu, M. K. Yoo, H. J. Jeong, H. J. Lee, M. Muthiah, J. H. Rhee, J. H. Lee, C. S. Cho, Y. Y. Jeong, I. K. Park, *Acta Biomater.* **2011**, *7*, 3935.
[160] M. G. Harisinghani, J. Barentsz, P. F. Hahn, W. M. Deserno, S. Tabatabaei, C. H. Van De Kaa, J. De La Rosette, R. Weissleder, *N. Engl. J. Med.* **2003**, *348*, 2491.
[161] D. L. J. Thorek, D. Ulmert, N.-F. M. Diop, M. E. Lupu, M. G. Doran, R. Huang, D. S. Abou, S. M. Larson, J. Grimm, *Nat. Commun.* **2014**, *5*, 3097.
[162] J. Zeng, B. Jia, R. Qiao, C. Wang, L. Jing, F. Wang, M. Gao, *Chem. Commun.* **2014**, *50*, 2170.
[163] D. Mahadevan, D. D. Von Hoff, *Mol. Cancer Ther.* **2007**, *6*, 1186.
[164] R. Kalluri, M. Zeisberg, *Nat. Rev. Cancer* **2006**, *6*, 392.
[165] R. F. Hwang, T. Moore, T. Arumugam, V. Ramachandran, K. D. Amos, A. Rivera, B. Ji, D. B. Evans, C. D. Logsdon, *Cancer Res.* **2008**, *68*, 918.
[166] D. Cantero, H. Friess, J. Deflorin, A. Zimmermann, M. A. Brundler, E. Riesle, M. Korc, M. W. Buchler, *Brit. J. Cancer* **1997**, *75*, 388.
[167] Y. Chen, B. Zheng, D. H. Robbins, D. N. Lewin, K. Mikhitarian, A. Graham, L. Rumpp, T. Glenn, W. E. Gillanders, D. J. Cole, X. H. Lu, B. J. Hoffman, M. Mitas, *Int. J. Cancer* **2007**, *120*, 1511.
[168] G. Y. Lee, W. P. Qian, L. Wang, Y. A. Wang, C. A. Staley, M. Satpathy, S. Nie, H. Mao, L. Yang, *ACS Nano* **2013**, *7*, 2078.
[169] J. Schwartzentruber, A. Korshunov, X.-Y. Liu, D. T. W. Jones, E. Pfaff, K. Jacob, D. Sturm, A. M. Fontebasso, D.-A. K. Quang, M. Toenjes, V. Hovestadt, S. Albrecht, M. Kool, A. Nantel, C. Konermann, A. Lindroth, N. Jaeger, T. Rausch, M. Ryzhova, J. O. Korbel, T. Hielscher, P. Hauser, M. Garami, A. Klekner, L. Bognar, M. Ebinger, M. U. Schuhmann, W. Scheurlen, A. Pekrun, M. C. Fruehwald, W. Roggendorf, C. Kramm, M. Duerken, J. Atkinson, P. Lepage, A. Montpetit, M. Zakrzewska, K. Zakrzewski, P. P. Liberski, Z. Dong, P. Siegel, A. E. Kulozik, M. Zapatka, A. Guha, D. Malkin, J. Felsberg, G. Reifenberger, A. Von Deimling, K. Ichimura, V. P. Collins, H. Witt, T. Milde, O. Witt, C. Zhang, P. Castelo-Branco, P. Lichter, D. Faury, U. Tabori, C. Plass, J. Majewski, S. M. Pfister, N. Jabado, *Nature* **2012**, *482*, 226.
[170] P. Ballabh, A. Braun, M. Nedergaard, *Neurobiol. Dis.* **2004**, *16*, 1.
[171] D. J. Begley, *Pharmacol. Ther.* **2004**, *104*, 29.
[172] G. Orive, O. A. Ali, E. Anitua, J. L. Pedraz, D. F. Emerich, *Biochim. Biophys. Acta, Rev. Cancer* **2010**, *1806*, 96.
[173] L. Wei, G. Zhou, Z. Li, L. He, M. Y. Gao, J. Q. Tan, H. Lei, *Magn. Reson. Imaging* **2007**, *25*, 1442.
[174] A. J. Carman, J. H. Mills, A. Krenz, D. G. Kim, M. S. Bynoe, *J. Neurosci.* **2011**, *31*, 13272.
[175] X. H. Gao, J. Qian, S. Y. Zheng, Y. Z. Changyi, J. P. Zhang, S. H. Ju, J. H. Zhu, C. Li, *ACS Nano* **2014**, *8*, 3678.
[176] C. H. Fan, C. Y. Ting, H. J. Lin, C. H. Wang, H. L. Liu, T. C. Yen, C. K. Yeh, *Biomaterials* **2013**, *34*, 3706.
[177] A. H. Mesiwala, L. Farrell, H. J. Wenzel, D. L. Silbergeld, L. A. Crum, H. R. Winn, P. D. Mourad, *Ultrasound Med. Biol.* **2002**, *28*, 389.
[178] T. Cedervall, I. Lynch, S. Lindman, T. Berggard, E. Thulin, H. Nilsson, K. A. Dawson, S. Linse, *Proc. Natl. Acad. Sci. USA* **2007**, *104*, 2050.

[179] C. D. Walkey, J. B. Olsen, F. Song, R. Liu, H. Guo, D. W. Olsen, Y. Cohen, A. Emili, W. C. Chan, *ACS Nano* **2014**, *8*, 2439.
[180] S. Tenzer, D. Docter, J. Kuharev, A. Musyanovych, V. Fetz, R. Hecht, F. Schlenk, D. Fischer, K. Kiouptsi, C. Reinhardt, K. Landfester, H. Schild, M. Maskos, S. K. Knauer, R. H. Stauber, *Nat. Nanotechnol.* **2013**, *8*, 772.
[181] A. Jedlovszky-Hajdu, F. B. Bombelli, M. P. Monopoli, E. Tombacz, K. A. Dawson, *Langmuir* **2012**, *28*, 14983.
[182] M. A. Dobrovolskaia, B. W. Neun, S. Man, X. Ye, M. Hansen, A. K. Patri, R. M. Crist, S. E. Mcneil, *Nanomedicine* **2014**, *10*, 1453.
[183] S. Barkam, S. Saraf, S. Seal, *Wiley Interdiscip. Rev.: Nanomed. Nanobiotechnol.* **2013**, *5*, 544.
[184] M. P. Monopoli, C. Aberg, A. Salvati, K. A. Dawson, *Nat. Nanotechnol.* **2012**, *7*, 779.
[185] S. M. Moghimi, Z. S. Farhangrazi, *Nanomedicine* **2013**, *9*, 458.
[186] M. A. Dobrovolskaia, A. K. Patri, J. Zheng, J. D. Clogston, N. Ayub, P. Aggarwal, B. W. Neun, J. B. Hall, S. E. Mcneil, *Nanomedicine* **2009**, *5*, 106.
[187] C. D. Walkey, W. C. W. Chan, *Chem. Soc. Rev.* **2012**, *41*, 2780.
[188] D. Docter, S. Strieth, D. Westmeier, O. Hayden, M. Y. Gao, S. K. Knauer, R. H. Stauber, *Nanomedicine* **2015**, *10*, 503.
[189] D. Docter, D. Westmeier, M. Markiewicz, S. Stolte, S. K. Knauer, R. H. Stauber, *Chem. Soc. Rev.* **2015**, *44*, 6094.
[190] C. Sacchetti, K. Motamedchaboki, A. Magrini, G. Palmieri, M. Mattei, S. Bernardini, N. Rosato, N. Bottini, M. Bottini, *ACS Nano* **2013**, *7*, 1974.
[191] K. Natte, J. F. Friedrich, S. Wohlrab, R. Von Klitzing, W. Osterle, *Colloids Surf., B* **2013**, *104*, 213.
[192] A. K. Murthy, R. J. Stover, W. G. Hardin, R. Schramm, G. D. Nie, S. Gourisankar, T. M. Truskett, K. V. Sokolov, K. P. Johnston, *J. Am. Chem. Soc.* **2013**, *135*, 7799.
[193] D. Pozzi, V. Colapicchioni, G. Caracciolo, S. Piovesana, A. L. Capriotti, S. Palchetti, S. De Grossi, A. Riccioli, H. Amenitsch, A. Lagana, *Nanoscale* **2014**, *6*, 2782.
[194] C. D. Walkey, J. B. Olsen, H. Guo, A. Emili, W. C. W. Chan, *J. Am. Chem. Soc.* **2012**, *134*, 2139.
[195] D. F. Moyano, K. Saha, G. Prakash, B. Yan, H. Kong, M. Yazdani, V. M. Rotello, *ACS Nano* **2014**, *8*, 6748.

Received: August 2, 2015
Revised: September 22, 2015
Published online: December 17, 2015